STUK

STUK-A196 / MAY 2003

OBJECTIVE MEASUREMENT OF IMAGE QUALITY IN FLUOROSCOPIC X-RAY EQUIPMENT: FLUOROQUALITY

M. Tapiovaara

STUK • **SÄTEILYTURVAKESKUS**
STRÅLSÄKERHETSCENTRALEN
RADIATION AND NUCLEAR SAFETY AUTHORITY

Osoite/Address • Laippatie 4, 00880 Helsinki
Postiosoite / Postal address • PL / P.O.Box 14, FIN-00881 Helsinki, FINLAND
Puh./Tel. +358 9 759 881 • Fax +358 9 759 88 500 • www.stuk.fi

The conclusions presented in the STUK report series are those of the authors and do not necessarily represent the official position of STUK

ISBN 951-712- 688-3 (print)
ISBN 951-712- 689-1 (pdf)

ISSN 0781-1705

Dark Oy, Vantaa 2002

Sold by:
STUK – Radiation and Nuclear Safety Authority
P.O. Box 14, FIN-00881 Helsinki, Finland
Phone: +358 9 759 881
Fax: +358 9 7598 8500

TAPIOVAARA Markku. STUK-A196. Objective Measurement of Image Quality in Fluoroscopic X-ray Equipment: FluoroQuality. Helsinki 2003, 50 pp. + apps. 13 pp.

Keywords medical imaging, x-ray imaging, fluoroscopy, image quality, statistical decision theory, ideal observer, quasi-ideal observer, detectability, signal-to-noise ratio, SNR, accumulation rate of the signal-to-noise ratio squared, SNR^2_{rate}, Wiener spectrum, spatio-temporal noise power spectrum, NPS, temporal lag, optimisation, quality control, measurement method, computer program

Abstract

The report describes FluoroQuality, a computer program that is developed in STUK and used for measuring the image quality in medical fluoroscopic equipment. The method is based on the statistical decision theory (SDT) and the main measurement result is given in terms of the accumulation rate of the signal-to-noise ratio squared (SNR^2_{rate}). In addition to this quantity several other quantities are measured. These quantities include the SNR of single image frames, the spatio-temporal noise power spectrum and the temporal lag. The measurement method can be used, for example, for specifying the image quality in fluoroscopic images, for optimising the image quality and dose rate in fluoroscopy and for quality control of fluoroscopic equipment. The theory behind the measurement method is reviewed and the measurement of the various quantities is explained. An example of using the method for optimising a specified fluoroscopic procedure is given. The User's Manual of the program is included as an appendix. The program is available free of charge for research work and program evaluation purposes by contacting the author.

TAPIOVAARA Markku. STUK-A196. Objective Measurement of Image Quality in Fluoroscopic X-ray Equipment: FluoroQuality. Helsinki 2003, 50 s. + liitteet 13 s. Englanninkielinen.

Avainsanat lääketieteellinen kuvantaminen, röntgenkuvantaminen, läpivalaisu, kuvanlaatu, tilastollinen päätöksentekoteoria, ideaalinen havaitsija, kvasi-ideaalinen havaitsija, havaittavuus, signaali-kohinasuhde, SNR, signaali-kohinasuhteen neliön kertymänopeus, SNR^2_{rate}, spatiotemporaalinen kohinan tehospektri, NPS, kuvan hitaus, optimointi, laadunvarmistus, mittausmenetelmä, tietokoneohjelma

Tiivistelmä

Raportti kuvailee STUKissa kehitettyä FluoroQuality-nimistä tietokoneohjelmaa, jota voidaan käyttää lääketieteellisten läpivalaisulaitteiden kuvanlaadun mittaamiseen ja analysointiin. Mittausmenetelmä perustuu tilastolliseen päätöksentekoteoriaan ja keskeisin mittaustulos on signaali-kohinasuhteen neliön kertymänopeus (SNR^2_{rate}). Kuvadatasta analysoidaan myös muita suureita, kuten yksittäisten videokuvien signaali-kohinasuhde (SNR), spatiotemporaalinen kohinan tehospektri ja kuvan hitaus (lag). Mittausmenetelmää voidaan käyttää esimerkiksi läpivalaisukuvan laadun ilmaisemiseen, läpivalaisun kuvanlaadun ja potilaan annosnopeuden optimointiin sekä läpivalaisulaitteiden laadunvarmistukseen. Raportissa on katsaus mittausten taustalla olevaan teoriaan ja eri suureiden mittausmenetelmät on selostettu. Esimerkkinä näytetään menetelmän käyttö erään läpivalaisututkimuksen optimoinnissa. Ohjelman käyttöohje on raportin liitteenä. Ohjelman käyttölisenssin saa tekijältä ilmaiseksi tutkimustarkoituksiin ja mittausmenetelmän käyttökelpoisuuden arviointiin.

Contents

1 Introduction

This report describes FluoroQuality, a computer program that is intended for the measurement of physical image quality in medical fluoroscopic equipment. The measurement method of the program is based on statistical decision theory (SDT), and fluoroscopic image quality is described primarily by the accumulating rate of the square of the signal-to-noise ratio (SNR) of the ideal (and a quasi-ideal) observer's decision variable. These SNR^2_{rate}:s relate to the detectability of a specified static detail in the image sequence by the ideal (or quasi-ideal) observer. The measurement is made by adding and removing the detail of interest in or from the phantom being imaged and analysing these recorded image data. By choosing the phantom so as to sufficiently mimic the scattering and attenuation of radiation in a patient, and choosing a detail that mimics a diagnostically important detail in the x-ray examination, the measurement should be closely related to the clinical quality of actual patient imaging. By varying the phantom and the detail to be detected, various detection tasks (see also Hanson 1983) can be considered, according to the x-ray examinations of interest. In addition to SNR^2_{rate} the program produces also other quality related data which should be useful in evaluating the performance of the imaging system and for constancy testing.

The phantom need not necessarily be homogeneous – in principle, also an anatomic phantom may be used. However, high-contrast phantom structures may violate the assumption of noise stationarity and therefore make the noise power spectrum measurements uncertain. Such phantom structures may also make the detectability of the detail dependent on its specific location in the phantom, and therefore achieving a good repeatability of SNR-results may be difficult. Therefore, it is recommended to use a homogeneous phantom for most measurement applications.

Unfortunately, because of the lack of a standard for recording image data, FluoroQuality is not presently a stand-alone program. Before one can use FluoroQuality to analyse the image sequences one must first record the image data digitally with a specified file format (see Appendix D). This recording of image sequences must be made by using another program, referred to as the acquisition program in this report. The acquisition program may record the sequences digitally from the analogue video signal by using a PC/frame grabber system or prepare the image data to be analysed from digital image sequence files of digital x-ray equipment. The FluoroQuality program then calculates and displays the ideal and quasi-ideal observers' SNR of single

frames, their SNR^2_{rate} of the acquired image sequences, the lag factor, and the noise power spectrum (NPS) of the acquired image data. The program also displays the average image for the signal and background situations, the net signal and the ideal observer's SNR^2 and SNR^2_{rate} spectra, and can be used for visualising the acquired image data.

2 Background

Only a short review of the concepts of image quality that are required as a background will be given here. It is not attempted to present the evolution of the ideas and concepts or to trace them to the original publications: for the original references and a more thorough and detailed presentation we refer to the scientific literature on the subject.

A general reference for the concepts of image measurements and image quality is the book of Dainty and Shaw (1974). Barrett and Myers (2003) present a thorough mathematical treatment of the subject. Books that consider specifically medical imaging are, e.g.: Barrett and Swindell (1981), ICRU (1996) and Beutel et al. (2000). Useful general textbooks on statistical decision theory are, e.g., Green and Swets (1966), van Trees (1968) and Whalen (1971).

2.1 General concepts of image quality

Imaging is basically a process consisting of two distinct stages: image recording and image display (Wagner 1983, ICRU 1996). This division is especially important in digital imaging, where these stages are clearly separate. In this case, when evaluating image quality, one must first decide what one means by the “image”: the acquired image data in the computer memory, or a given displayed version of the data. Here, the word “image” refers to the acquired image data.

For discussing image quality, one also needs to define “quality”. Images are used for various purposes. This suggests that, in order to define the concept of image quality in a reasonable manner, the underlying task of using the image should be specified: an image can be defined to be of good quality if it fulfils its intended task well. Image quality then becomes a task-dependent quantity; images ranked by one imaging task will not necessarily rank similarly in another task. For example, if the visibility of small-sized details is important, imaging system performance at high spatial frequencies may be a more important factor than imaging system performance at low spatial frequencies, and vice versa if the visibility of large, low-contrast objects is required (ICRU 1996).

It could be thought that such a definition of image quality would obscure matters: image quality is then not solely dependent on image properties, but also on the detection task, the observer’s a-priori information on the task and the observer’s ability to use both the prior information and the image

information for his decisions. This apparent difficulty cannot be avoided, but can be dealt with by specifying the task and the observer in detail.

The problem of prior information is commonly treated by considering the case of full a-priori information: the observer is given all information on the expected signal and background, the signal transfer properties of the imaging system and the properties of the image noise. The only thing that the observer does not know a-priori is whether the signal is in the image or not[*)]: the observer's task is to make a decision on the signal's presence. The detection experiment is repeated many times and image quality is measured statistically by observing how many errors (false positives and false negatives) the observer makes. The less detection errors the observer makes, the better the image quality is. This performance can be summarised by the observer's SNR at the decision stage: it describes the accuracy of the the observer in classifying images with and without the signal to the correct signal and background classes.

It would not be of much interest to study how an unskilled or inefficient observer would succeed in detecting the signal: the results would describe more the observer's (in)ability than the actual information in the images. In order to get a unique performance figure which describes the actual quality of the image data in an absolute scale one uses the best possible observer (the ideal observer) for observing the images. This observer uses all the information in the images and all available prior information in the optimal way to make its decision. The ideal observer then achieves the lowest detection error rate that is possible by using the image data. Therefore, the performance of the ideal observer is a measure of the amount of information in the image which is relevant to the specified imaging task.

In an SKE/BKE task any decision errors that the ideal observer makes result from the image quality not being perfect; full prior data is given to the observer. One must be cautious in interpreting the SKE/BKE data, however, because sometimes the detection task may become too tightly specified and not anymore correspond to the actual detection task of interest. An example of such a case is given by Myers et al. (1990).

The ideal observer is well known in the SKE/BKE task, when the image noise is signal-independent and normally distributed, and can be realised as a prewhitening matched filter (Wagner and Brown 1985)[**)]. In practical

[*)] This task is often also referred to as the SKE/BKE (signal-known-exactly/background-known-exactly) task.

[**)] When there is less prior information on the detection task, the ideal observer becomes mathematically more complicated. An example of this is given in Brown et al. (1995), where the case of unknown signal position was considered.

measurements it is not always necessary to use this strictly ideal observer, but one can be content of using a close approximation of it, a quasi-ideal observer, which may be easier to implement in practice. In FluoroQuality image quality is assessed by estimating the SNR of both the ideal observer and a quasi-ideal observer (Tapiovaara and Wagner 1993).

The above discussion is related to the image quality in general detection tasks. In medical imaging the image is used as a means to get information of the health status of the patient, and ultimately, clinical image quality should be evaluated by the impact of the image to a correct diagnosis or to the outcome of the treatment of the patient (ICRU 1996). The evaluation of clinical performance is extremely cumbersome, however, and the results depend not only on the image quality, but also on the skills of the diagnosticians interpreting the images and the patient material. Therefore, the calibration of patient-image-based quality assessments is unclear and the results can hardly be accurately reproduced by others. Simpler imaging tasks are thus required for the measurement and reporting of image quality in radiology. One possibility is to use patient simulating phantoms, and base the measurement on the detectability of phantom details that resemble important disease-related structures in actual patients. If the phantom is designed carefully, it should be credible that the detectability of these details in phantom images is related to the detectability of important features in actual patient images, and thus to the achievable accuracy in diagnostics.

2.2 Basic factors of image quality: MTF, contrast and NPS

Physical image quality depends on several factors. The most important of these are image sharpness, contrast and noise. Other factors, such as image distortions, homogeneity and artefacts may be important, too, but are not treated here. They are usually of less importance in conventional x-ray imaging than the former and can be often corrected in the final image, at least in principle. In a sense, image noise is the most important quality-limiting factor in radiological imaging, because it sets limits to the detectability of details – and also restricts possibilities to get the details visible by image enhancement (e.g., image sharpening and contrast increase). Image noise is unavoidable in medical x-ray imaging if the dose to the patient is to be kept low.

The sharpness of images is often evaluated visually by the resolution seen in line-pair test object images. The sharpness of linear shift-invariant imaging systems can be better described by measuring the modulation transfer function (MTF, see, e.g., ICRU 1986). The measurement may sometimes be

straightforward, at least in principle, but is usually complicated by problems caused by noise, the low intensity of the image signal from the thin slit or small aperture used for the measurement, and the wide dynamic range needed in measuring the line spread function or point spread function.

A further difficulty, especially in electronic imaging, is that the isotropy of the imaging system is not granted and the determination of the full two-dimensional MTF may be necessary. In fluoroscopy the situation is even more complex, because time (or temporal frequency) constitutes a third dimension to the measurement, and relates to the temporal blurring of the signal (i.e., lag). So far, no practical methods for measuring the spatio-temporal MTF of dynamic imaging systems have been presented in the literature.

The measurement of the MTF in digital imaging systems is further complicated by the fact that these systems are not necessarily shift-invariant at scales of the order of the pixel size (Dobbins 1995). Therefore, the MTF of digital equipment is usually reported in terms of the presampling MTF, which does not consider the effect of the discrete sampling on the image.

In addition to the MTF, the other factor needed for describing the signal transfer in the imaging chain is the contrast transfer. Image contrast results from the radiation contrast of the detail and the large area transfer characteristics of the imaging system (such as the characteristic curve of x-ray film). The measurement of the large area transfer characteristics (sensitometry) should be relatively simple, but the determination of the radiation contrast of the detail may be difficult: it depends, e.g., on the x-ray spectrum, the attenuation of the radiation in the phantom (or patient) and in the detail considered, the amount of scattered radiation in the image and the photon energy response of the image receptor.

Image noise is often evaluated visually by determining the threshold contrast. Mathematically, the image noise of stationary imaging systems can be characterised by the noise power spectrum (NPS, Wiener spectrum). In projection radiography the NPS represents the noise power at various spatial frequencies (specified by f_x and f_y, the horizontal and vertical spatial frequencies). In fluoroscopy the NPS is three-dimensional: in addition to the spatial frequency co-ordinates one must also specify the noise power as a function of temporal frequency (Goldman 1992, Tapiovaara and Wagner 1993, Tapiovaara 1993, Cunningham et al. 2001, Siewerdsen et al. 2002). It can be noted that the 2D spatial NPS of the individual images in the image sequence can be obtained by integrating the 3D spatio-temporal NPS of the sequence over the temporal frequency. In FluoroQuality both the 3D spatio-temporal NPS and the 2D spatial NPS of single image frames are measured. The

equations for NPS measurement as used in FluoroQuality are given in Chapters 3.4 and 3.5.

There are ambiguities in noise measurements, too. For example, any non-homogeneity in the image background, originating from the non-homogeneity in the phantom or the image receptor, is often considered as being noise. This is reasonable if the observer does not know these structures and the structures actually vary from one image to another*). If the spatial variability stays constant in all images one cannot treat it as being random, although the detailed structure of the non-homogeneity would be unknown to the observer.

In practice, the noise analysis is often made by subtracting a constant brightness value or a slowly varying fit from the image data before calculating the NPS. This corresponds to considering other brightness variability as being noise, and may result to false anomalous NPS values if the background structure does not change between analysed image samples. In FluoroQuality another alternative is used: the noise is analysed from image samples obtained from the same location of the image receptor after subtracting the actual averaged image from the samples. Background variability is then treated as being a deterministic, known structure, which does not impair detail detectability. This may not always be realistic for a human observer, who may in some cases suffer from background variability more than from actual stochastic noise (Kotre 1998, Bochud et al. 1999, Burgess et al. 2001a and b, Marshall et al. 2001), but is certainly applicable to the ideal observer. Human observers seem to operate somewhere between the two interpretations: background variability appears to function as a mixture of noise and deterministic masking components. For a more detailed discussion on this matter, see, e.g., Burgess et al. (2001b) and the references therein.

In FluoroQuality the measurement of signal transfer characteristics is not attempted and only the visibility of static details is considered. Instead of using a model of the signal and its transfer, the mean detail image is obtained directly as the difference of averaged (almost noiseless) images that are acquired with and without the signal detail in the phantom. This difference image automatically contains all the factors that affect either image sharpness or contrast. As already stated above, the spatio-temporal NPS is measured, however, and is displayed as 2D cuts at different temporal frequencies.

*) However, especially in the case of unknown anatomical background, the variability does not necessarily conform with the underlying assumptions of NPS analysis (noise stationarity and ergodicity).

2.3 Summary measures of image quality: SNR, NEQ and DQE

Presently, image quality assessment in medical imaging is most often based on the statistical decision theory (or signal detection theory, SDT) and uses quantities such as the ideal observer's signal to noise ratio (SNR_{ideal}), noise equivalent quanta (NEQ) and detective quantum efficiency (DQE). The applicability of this approach for several medical imaging modalities was summarised by Wagner and Brown (1985) and has been reviewed in ICRU (1996).

In digital imaging systems, images can be easily manipulated: e.g., their brightness and contrast can be changed and images can be spatially filtered to suppress noise or improve sharpness. Therefore, the factors MTF, NPS and contrast transfer are not of much use in digital imaging if one of them is used alone without reference to the others. For example, the MTF can be adjusted to almost any shape by filtering the image. Such filtering affects also the NPS, however, and therefore, a summary measure combining these factors properly (such as SNR, NEQ or DQE) is required for describing the system performance. The same applies to contrast, which can be manipulated in electronic imaging systems to an arbitrary degree, but affects both the signal and the noise.

In the SDT framework, image quality assessment applies to the image data stage, and describes the performance of a specified (mathematical) observer when it analyses images. The observer calculates a decision variable which describes the observer's confidence for the presence or absence of the specified detail in the image (an image will be denoted by the symbol g). Detection performance is measured statistically on an ensemble of images, and is described by the separability of the conditional distributions of the decision variable, $D(g \mid s)$, for the signal and background cases. The overlapping of these distributions specifies the probability of both types of detection errors, false alarms and misses, and can be presented by the observer's receiver operating characteristic (ROC) curve. Frequently, this separability of the distributions is reported in terms of the separation of their means divided by their standard deviation; this is the observer's signal-to-noise ratio

$$SNR = \frac{\left| \overline{D(g \mid signal)} - \overline{D(g \mid background)} \right|}{\sigma_D}. \qquad (1)$$

The SNR-description is sufficient for specifying the observer's performance when the conditional distributions of the decision variable are normally distributed and have equal variance for both, the signal and background cases.

For the evaluation of the physical or technical quality of images or imaging systems, the ICRU report (1996) suggests the measurement of the large scale system transfer function (in linear systems the gain, *K*), the modulation transfer function (*MTF*) and the noise power spectrum (NPS: symbol *W*). These measurements are then combined to obtain the noise equivalent quanta (*NEQ*), the detective quantum efficiency (*DQE*), or the ideal observer's signal-to-noise ratio (SNR_{ideal}) for a specified signal Δs.

The *NEQ* of a linear imaging system is defined as

$$NEQ(f_x, f_y) = \frac{K^2 \cdot MTF^2(f_x, f_y)}{W(f_x, f_y)} . \tag{2}$$

Spatial frequency *f* is expressed here by its horizontal and vertical components, f_x and f_y, because images are two-dimensional objects. NEQ can be interpreted as the number of quanta (actually: photon fluence) at the input of a perfect detector that would yield the same output noise, as a function of spatial frequency, as the real detection system under consideration. In other words, NEQ expresses the quality of the image data by the photon fluence that the image is worth at each spatial frequency.

By comparing the *NEQ* with the actual photon fluence, *Q*, used for forming the image, one obtains the *DQE*:

$$DQE(f_x, f_y) = \frac{NEQ(f_x, f_y)}{Q}, \tag{3}$$

which can be interpreted as expressing the efficiency with which the imaging system has utilised the available photons: for a perfect system *DQE = 1* for all spatial frequencies. DQE expresses, therefore, rather the quality of the equipment and the efficiency of radiation use than the quality of the image itself: a low dose radiograph is bound to be noisy and, therefore, of not high quality, although the DQE may be high.

The SNR_{ideal} for a specified SKE/BKE-detection task, described by the difference of the signal and background inputs, $\Delta s(x,y)$, can be calculated as

$$SNR_{ideal}^2 = \iint \frac{K^2 MTF^2(f_x, f_y) \left|\Delta S(f_x, f_y)\right|^2}{W(f_x, f_y)} df_x df_y , \tag{4}$$

where $\Delta S(f_x,f_y)$ is the Fourier transform of $\Delta s(x,y)$.

One can also express the DQE as a task-related quantity, as

$$DQE = \frac{SNR^2_{ideal,image}}{SNR^2_{ideal,in}}, \quad (5)$$

where $SNR^2_{ideal,\,image}$ and $SNR^2_{ideal,\,in}$ relate to the detectability of a given detail, as based on the image data and the radiation incident on the image receptor, respectively (Tapiovaara and Wagner 1985).

The above equations (2–4) have been written here for the case of analogue images. A treatment involving the discrete pixels of digital imaging modalities has been used, for example, in ICRU report 54, Myers et al. (1987) and Tapiovaara and Wagner (1993). In this treatment, images are represented by vectors whose dimensionality corresponds to the number of pixels in the image.

Digital imaging poses some problems for NEQ and DQE measurements (Dobbins 1995, Pineda and Barrett 2001, Gagne et al. 2001a and b). The main problem is undersampling, which, when present, results to aliasing. The MTF is then no longer a transfer factor of a given frequency. Aliasing can also be described as the consequence of the violation of the assumption of shift-invariance, which would be required in the MTF-analysis: the image of a point may depend on the actual location of the point with respect to the pixel boundaries.

One possible solution for measuring the “MTF” in such a system is to locate the stimulus at all possible locations within the pixel boundaries (this can be done using, e.g. a slightly angulated slit), and calculate the average of these different MTFs. However, this average digital MTF then no longer is related to the point spread function at any location, and strictly cannot be used for comparing the sharpness of two systems. Another possibility is to measure the presampling MTF (Fujita et al. 1989). Dobbins (1995) concludes that in the common case of undersampled digital imaging, the interpretation of NEQ is difficult and depends on the measurement method and the frequency content of the incident information. He suggests the use of the averaged digital MTF for calculating the NEQ. In other publications, variable definitions of NEQ have been used, but the use of the presampling MTF seems to become the most common convention. However, there is no unambiguous solution for interpreting the NEQ or DQE results at frequencies where aliasing effects are important.

The above problem can be avoided in measuring the SNR: if the SNR measurement is done more directly, not by going through the transfer function analysis, but by measuring the detectability of the detail as based on how the detail is actually imaged, the problem is circumvented. It is noted that the nominator in Eq. (4) represents the expected image signal

$$(6) \qquad \left|\Delta G(f_x, f_y)\right| = K \cdot MTF(f_x, f_y) \cdot \left|\Delta S(f_x, f_y)\right|.$$

This expected image signal can be directly obtained also from the difference of averaged background and signal images: the directly measured ΔG can be used instead of both the system transfer characteristics and the signal model in Eq. (4). In digital images the ideal observer's SNR can then be obtained as the sum

$$(7) \qquad SNR^2_{ideal} = \sum_f \frac{\left|\Delta G_f\right|^2}{W_f},$$

where ΔG_f is the signal spectrum at spatial frequency $f = (f_x, f_y)$ and W_f is the f-th component of the noise power spectrum. We shall refer the factors $SNR^2_f = |\Delta G_f|^2 / W_f$ to as the ideal observer's SNR^2-spectrum – it shows the contribution of each spatial frequency component to the total SNR^2_{ideal}.

The practical difficulty of measuring SNR_{ideal} with this approach is in obtaining a sufficient number of images for the averaging, so that the error from residual noise would be small (Gagne and Wagner 1998). In addition to the random variability in the results, the residual noise also causes a positive bias to the SNR-estimate. According to the theory of Gagne and Wagner this bias depends on the number of image samples and the biased estimate of the SNR^2-spectrum can be corrected to a de-biased estimate by

$$(8) \qquad SNR^2_{f,debiased} = \left(\frac{2N-3}{2N-2}\right) SNR^2_{f,biased} - \frac{2}{N},$$

where N denotes the number of signal and background image samples in the measurement (total number of images is 2·N). The bias is slightly different at the zero frequency and at the Nyquist frequency (the factor in the parentheses is $(N–2)/(N–1)$ for these frequencies). FluoroQuality displays the de-biased SNR^2-spectra related to both the individual image frames and to the temporal zero-frequency [corresponding to SNR^2_{rate} and the detectability of a static detail in the fluoroscopic sequence (to be explained later in the text)]. The program

also reports the de-biased SNR^2 and SNR^2_{rate} calculated from Eq. (8); the data are calculated as the sum over various frequency ranges.

Another possibility of measuring the SNR is not to use the mathematical relationships between the SNR and its constituents (Eqs. 4 or 7), but to actually construct the mathematical observer and let it make decisions on the detail presence in images with and without the signal detail in the phantom. This approach will be considered in more detail later.

If the measurement is done in either of these ways, the result may depend on the exact position of the detail with respect to the pixel array if aliasing phenomena are present, and thus vary somewhat from one measurement to another. If necessary, a solution to this is to make several SNR-measurements with small shifts in the detail position and report the mean detectability. Pineda and Barrett (2001) also discuss this solution. In their simulations they found that a direct SNR-measurement from the digital data is necessary when the signal size is of the order of, or smaller than a pixel – both of the approximate solutions (using the averaged digital MTF or the presampling MTF) can result to erroneous conclusions of system performance.

In measuring the SNR, it may not always be necessary to consider the strict ideal observer. Other computational observers, such as the non-prewhitening matched filter (NPWMF, Wagner and Brown 1985), perceived statistical decision theory model (Loo et al. 1984), the NPWE model (Burgess et al. 2001b), the Hotelling observer (Smith and Barrett 1986), the channelized ideal observer (Myers and Barrett 1987), the DC-suppressing observer (Tapiovaara and Wagner 1993) and the DCsHFs-observer who suppresses the information in two isolated spatial frequencies (0, 0) and (0, v_{max})[*)] (Tapiovaara 1997) have been suggested for sub-optimal alternatives, among others. A number of publications (e.g., Loo et al. 1984) have shown the close relationship between the performance of such observers and human observers.

The DC-suppressing observer has been used for measuring image quality in fluoroscopy by a PC/frame grabber system in laboratory (Tapiovaara 1993) and clinical (Tapiovaara et al. 2000) settings, and for image quality measurement in a digital radiography system (Gagne et al. 2001a). A related methodology has also been applied for evaluating phantom images in mammography (Chakraborty 1996 and 1997) and the measurement of the

[*)] This observer can be called the DCsHFs-observer, because it suppresses both, the spatial DC frequency and the maximum vertical frequency. The noise may often be excessive at the DC channel, and the same is often true for the frequency (0, v_{max}) for interlaced imaging systems. Including these uncertain channels in calculating the quasi-ideal observer's information may impair its performance unnecessarily. A similar approach can be used also in other cases where there are isolated frequencies with excessive noise.

displayed image quality in display devices by using a CCD camera to view the display (Chakraborty et al. 1999a). In these methods, the measurement of MTF, NPS or K is not needed, but the measurement can be performed simply by applying the DC-suppressing observer's detection algorithm to images that are acquired both with and without the detail object in the phantom. The DC-suppressing observer is constructed by first obtaining (e.g. by averaging of a large number of images) approximately noiseless reference images of the phantom in both cases, the detail present in the phantom and the detail removed. Then, by denoting the difference of these averaged images by Δg, the decision function is obtained as

$$D_{DCS}(g) = \sum_{i,j} \left[\Delta g_{i,j} - \frac{1}{P} \sum_{k,l} \Delta g_{k,l} \right] g_{i,j} \tag{9}$$

where $g_{i,j}$ denote the pixel values of each image analysed for signal presence and P is the number of pixels in the image area analysed. The SNR is estimated from a set of signal and background images as shown in Eq. (1). An advantage of this method is that the result is not based on any model of observer performance, but represents the performance of an actual observer. The result may not always be a good estimate of the ideal observer's performance, however. The ideal observer would outperform it notably if the signal is spread to frequencies where the NPS is strongly frequency dependent. This may also be the case in signal-dependent (non-additive) noise situations where the ideal observer's strategy differs from the filtering scheme described above.

The above method (Eqs. 1 and 9) applies to static x-ray images. To measure the information relevant to the detail detectability in fluoroscopy, one must determine the accumulation rate of SNR^2 (SNR^2_{rate}). This quantity is the live-image analogy of SNR^2 in static imaging, and is required in fluoroscopy because the information obtained depends on the length of the image sequence; in fluoroscopy, the SNR^2 in a (reasonably long*)) image sequence is equal to SNR^2_{rate} multiplied by the imaging time. There are at least two approaches to measure this quantity. One is to record reasonably long fluoroscopic sequences (of a duration from one to a few seconds), to calculate the time-averaged mean images, calculate the SNR to a set of such averaged images, and finally divide the SNR^2 by the acquisition time. The other method involves the measurement of the single-frame SNR as for static radiographs above, and calculating the

*) In principle, this relationship holds also for short image sequences, but the difficulty then is in defining the imaging time; temporal lag spreads information to nearby image frames, and the imaging time is not equal to the number of image frames multiplied by the nominal frame duration.

SNR^2_{rate} by multiplying $SNR^2_{single\ frame}$ by the noise lag factor F (Tapiovaara 1993, see also Cunningham et al. 2001). This factor is calculated from the spatio-temporal NPS of the image sequence, and expresses the effective number of independent image frames per unit time. Because of lag, this number is usually smaller than the frame rate in the fluoroscopic system. SNR^2_{rate} is calculated by both these methods in FluoroQuality. The first method is more straightforward, but may suffer from the imprecision caused by the small number of image sequences analysed. In the image data system of FluoroQuality the number of analysed image frames is 32 times higher than the number of image sequences, and we expect that the precision obtained with the latter method is better.

In addition to the aliasing problems discussed earlier, these direct SNR-measurement methods provide also a solution to a further problem in NEQ- and DQE-like quantities: these latter quantities inherently apply only to imaging where a detail object affects only the *intensity* of the radiation and leaves the x-ray spectrum behind the detail unchanged (Tapiovaara and Wagner 1985 and 1993, Cahn et al. 1999). In x-ray imaging the detail of interest modifies also the x-ray spectrum shape. Therefore, when optimising the x-ray imaging conditions (for example the x-ray spectrum), it is not sufficient to consider only NEQ or DQE, but one must consider the spectral dependence of radiation contrast as well, and include it in the factor $\Delta S(f_x, f_y)$ above. Spectral dependence is properly and automatically taken care of by the direct SNR measurement methods.

We make here one last note considering DQE. The main application of this quantity is to describe the efficiency of *the image receptor*. Therefore, in the calculation of DQE, the number of noise equivalent quanta is compared to the actual number of quanta impinging on the image receptor. This is not directly the optimisation problem that is of interest in x-ray imaging. The efficiency in x-ray imaging is better described by comparing the achieved image quality (as related to the chosen task) to the dose in the patient. Therefore, in many papers discussing optimal imaging conditions, the optimisation process is based on maximising the efficiency of radiation use in terms of the dose-to-information conversion factor: SNR^2/dose or SNR^2_{rate}/dose rate (for example Tapiovaara et al. 1999, Chakraborty 1999b). This quantity helps in finding the most efficient conditions of imaging, but even this is not sufficient by itself: one also needs to decide on the image quality (i.e. actual details and their detectability) that is needed, and to work at the lowest dose level at which this quality can be obtained. In choosing the appropriate image quality level, one must then weigh the potential risk from the loss of diagnostic information in the low dose application against the larger radiation risk from higher dose techniques (Martin et al. 1999).

2.4 Visual assessment

Metz et al. (1995) have reviewed the assessment of medical image quality, and noted that there exists a wide consensus in measuring the sensitometric quantities, MTF and NPS of radiological systems. They also agreed that the combined measures NEQ, DQE and SNR_{ideal} (the ideal observer's signal-to-noise ratio) are useful for normalising the measurements on an absolute scale and for relating those measurements to the decision performance of the ideal observer. However, they stress that in the two-stage (recording and display) description of the imaging process, SNR_{ideal} describes image quality at the stage of image recording. This can be considered an advantage for understanding the steps through which images are formed, but the data stage cannot be used *alone* to predict the ranking of images that a human might make on basis of the displayed image if the characteristics between the images are too different. In many cases, however, such as projection radiography, the human and ideal observer results show a good correlation, and it seems that the efficiency of human observers is of the order of 50%. Similar observations have been made also in fluoroscopic imaging with image sequences replayed in a continuous loop; human efficiency was found to be 30–40% when the display contrast gain was sufficiently high (Tapiovaara 1997). In some other cases, for example, when comparing images where the observer's efficiency is different (e.g., because of different contrast or noise texture) the ranking of the images by a human observer's performance may differ from the ranking predicted by the SNR_{ideal}-measurement.

Human performance is not well understood for many clinically relevant tasks, and the relevance of the above objective measurements to human observer performance is not clear in all cases. Metz et al. (1995) stress that the assessment of medical imaging systems requires going also beyond phantom/laboratory measurements into the clinical setting, where clinical performance can be assessed by ROC-studies, for example. The same conclusions have been reached in ICRU (1996). It is also noted that even good quality image data can be easily spoiled at the display stage. Therefore, it is almost a necessity that images are also assessed visually at some stage of the evaluation process.

There are several ways with which a visual evaluation of image quality can be made – with a varying degree of sophistication. Presently, the Receiver Operating Characteristic (ROC) and Multiple Alternative Forced Choice (MAFC) tests are considered to be the best methods of obtaining quantitative and (in a less strict sense of the word) objective results of human observers' ability to detect signals in the images. The results from these tests can be given in terms of the decision-stage SNR of human observers, which is often denoted

as *d'*. These psychophysical methods can be used for both clinical studies of actual patient images and detection tests using simple phantom radiographs, but they are not suitable for, e.g., routine quality assurance work. Therefore, more simple but less accurate methods need often be used, e.g., subjective assessment of detail detectability in phantom images.

Often these phantoms and details are highly simplified, and the detection task may not be reasonably related to clinically meaningful tasks. Typical examples of common image quality measurement tools are line-pair test plates and contrast detail phantoms, whose images are visually evaluated. For a more detailed discussion on visual evaluation methods see, for example, ICRU Report 54, and the references therein.

3 The image quality quantities measured with FluoroQuality

3.1 Notation and conventions

FluoroQuality analyses only a part of the whole image area. The analysed area (sub-image) is selected in the acquisition program by the user. These sub-images must be of size 64x64 pixels, with 8-bit pixel depth, and each recorded sequence must contain 32 consecutive image frames. These image data are denoted below by $g_s(i, j, k, m)$, where i denotes the pixel column ($1 \le i \le 64$), j the pixel row ($1 \le j \le 64$), k the frame number ($1 \le k \le 32$) and m ($1 \le m \le M$) identifies the image sequence. (The number of image sequences, M, is determined in the acquisition program; values of $M \ge 40$ are recommended for keeping the bias and uncertainty small.) The subscript $s = 1$ for images recorded with the signal detail in the phantom, and $s = 0$ for images recorded with the detail removed.

Two- and three-dimensional discrete Fourier transformed (DFT) images are denoted with capital letters, and the horizontal, vertical and temporal frequencies are denoted by u, v and w, respectively: e.g., $G_s(u, v) = F_2[g_s(i, j)]$ and $G_s(u, v, w) = F_3[g_s(i, j, k)]$, where $F_n[]$ denotes the n-dimensional DFT operation. It is emphasized that FluoroQuality uses the symmetric normalisation convention of DFT; therefore, the transformation differs from the DFT with the (more commonly used) unsymmetrical normalisation convention by the factors $\sqrt{64 \cdot 64}$ and $\sqrt{64 \cdot 64 \cdot 32}$ for the 2D and 3D cases, respectively.

The width and height (in units of length) of the analysed 64x64 pixel sub-image is denoted as X and Y, respectively. However, X and Y are not actually measured in FluoroQuality and a numerical value of 1 is used for both of them. If the user wishes to express the spatial frequencies and the NPS in proper units (mm^{-1} and mm^2) the values of X and Y can be taken into account by hand calculation: for example, the horizontal frequency u ($-31 \le u \le 32$) corresponds to the spatial frequency u/X, and the 2D NPS values can be obtained by multiplying the values calculated in FluoroQuality by XY. The temporal length of the 32-frame image sequences is denoted as T.

One should also note that all values in FluoroQuality are calculated in terms of the pixel values. If the user so wishes, these values can be later converted to correspond to some other quantities, e.g., x-ray fluence, by applying the proper conversion factors. Such a conversion makes a difference only in the numerical values of the average images and NPS data – the signal-to-noise measures are not affected.

3.2 Average images

FluoroQuality calculates the average signal and background images (recorded with and without the signal detail in the phantom, respectively) as

$$\bar{g}_s(i,j) = \frac{1}{32 \cdot M} \sum_{m=1}^{M} \sum_{k=1}^{32} g_s(i,j,k,m), \quad s = \{0, 1\}. \tag{10}$$

The average images for the signal and background cases are shown on the FluoroQuality display form.

3.3 The net signal and its frequency spectrum

The net signal is obtained as

$$\Delta g(i,j) = \bar{g}_1(i,j) - \bar{g}_0(i,j) \tag{11}$$

and the spatial frequency spectrum of the signal is defined*) as

$$\left| \div G(u,v) \right|^2 \; | \; \left| F_2 \Psi g(i,j) \beta \right|^2. \tag{12}$$

The net signal image and the signal spectrum are shown on the FluoroQuality display form.

*) The relationship between this signal spectrum and the one used in eq. (7) is similar to the relationship between the noise quantities R and W in eq. (14).

3.4 The NPS of individual image frames and the spatio-temporal NPS at zero temporal frequency

The variance at each spatial frequency, $R(u, v)$, which is related to the two-dimensional NPS (see, e.g., Tapiovaara and Wagner 1993), is measured as

$$R_s(u,v) = \frac{1}{(M-1)}\left(\sum_{k,m} \left| F_2\{g_s(i,j,k,m)\} \right|^2 - \frac{1}{M} \left| \sum_{k,m} F_2\{g_s(i,j,k,m)\} \right|^2 \right). \quad (13)$$

The two-dimensional NPS corresponding to individual frames is then calculated as

$$W_{2D,s}(u/X, v/Y) = \frac{XY}{64^2} \cdot R_s(u,v). \quad (14)$$

The measurement is made separately for both the signal (s = 1) and background images (s = 0). When reporting the NPS, FluoroQuality uses the value 1 for both factors X and Y. If the user wishes to normalise his/her data to the actual size of the image, the calculated NPS-values should be multiplied with the measured value of XY, and the spatial frequencies are obtained by dividing the displayed (integer) values of u and v by X and Y, respectively. It is again emphasized that the normalisation in (14) differs from some other texts because of the DFT normalisation used; the resulting NPS is the same, however.

Similarly, the variance of the summed 32-frame long sequences, corresponding to the zero temporal frequency component of the 3D spatio-temporal NPS, is measured as

$$R_{sum,s}(u,v) = \frac{1}{M-1}\left(\sum_m \left| F_2\left\{ \sum_k g_s(i,j,k,m) \right\} \right|^2 - \frac{1}{M} \sum_m \left| F_2\left\{ \sum_k g_s(i,j,k,m) \right\} \right|^2 \right) \quad (15)$$

and the corresponding zero frequency component of the 3D spatio-temporal NPS of the sequences is calculated as

$$W_{3D,s}(u/X, v/Y, 0) = \frac{XYT}{64^2} \cdot R_{sum,s}(u,v). \quad (16)$$

Again, the measurement is made separately for both the signal (s = 1) and background images (s = 0), and the value 1 is used for the factors X, Y and T in the displayed data. Therefore, if the user wishes to normalise his/her data to the actual size of the image and the temporal length of the sequence, the calculated NPS-values should be multiplied with the measured value of XYT. The spatial frequencies are obtained by dividing the (integer) values of u and v by X and Y, respectively.

3.5 The full spatio-temporal NPS

The full spatio-temporal NPS is calculated as

$$W_{3D,s}(u/X, v/Y, w/T) = \frac{XYT}{(M-1)\cdot 64^2 \cdot 32} \sum_m \left| F_3\left[g_s(i,j,k,m) - \bar{g}_s(i,j) \right] \right|^2 . \quad (17)$$

Again, the measurement is made separately for both the signal (s = 1) and background images (s = 0), and the value 1 is used for the factors X, Y and T. If the user wishes to normalise his/her data to the actual size and temporal length of the image sequence, the calculated NPS-values should be multiplied with the measured value of XYT, and the spatial frequencies are obtained by dividing the (integer) values of u and v by X and Y, respectively. In displaying the NPS, the temporal length of the image sequences is already taken into account, and the proper temporal frequency (in Hz) is displayed on the NPS display-form.

3.6 The SNR-measures obtained by integration (analytical biased data)

Using the measured signal spectrum and NPS, FluoroQuality estimates the (biased) SNR^2 and SNR^2_{rate} of two computational observers: the DC- and HF-suppressing observer (DCsHFs) and the prewhitening matched filter (PWMF, the ideal observer). It should be noted that the residual noise in the average images and NPS data make these estimates high-biased, as discussed earlier in Chapter 2.3, and it is not advisable to use them for estimating the detectability of the signal. The data may be useful, however, for estimating the effect of the different detection algorithms on the resulting SNR estimate. The data are presented as a function of the maximum included spatial frequency in the summation, f_{lmt}.

The SNR^2_{DCsHFs} of the individual image frames is calculated as

$$SNR^2_{DCsHFs}(f_{lmt}) = \frac{\left(\sum_{f \neq (0,0) or (0,32)} \left| \Delta G(u,v) \right|^2 \right)^2}{\sum_{f \neq (0,0) or (0,32)} \tfrac{1}{2} \cdot \left(R_0(u,v) + R_1(u,v) \right) \left| \Delta G(u,v) \right|^2} , \quad (18)$$

where the summation is done only over frequencies $f = (u, v)$ where

$$|f| = \sqrt{u^2 + v^2} \leq f_{lmt} \quad (19)$$

and f_{lmt} is equal to 7, 15, 30 or not limited ($-31 \leq u, v \leq 32$).

The ideal observer's (biased) SNR^2 is calculated as

$$SNR^2_{PWMF}(f_{lmt}) = \sum_{f \le f_{lmt}} \frac{\left|\Delta G(u,v)\right|^2}{\tfrac{1}{2} \cdot \left(R_0(u,v) + R_1(u,v)\right)}, \tag{20}$$

and again presented as a function of the maximum included frequency, f_{lmt}.

In a close analogy of the above formulae, the SNR^2_{rate} of the observers is calculated as

$$SNR^2_{rate,DCsHFs}(f_{lmt}) = \frac{1}{T} \cdot \frac{\left(\sum_{f \neq (0,0) or (0,32)} \left|\Delta G(u,v)\right|^2 \right)^2}{\sum_{f \neq (0,0) or (0,32)} \tfrac{1}{2} \cdot \left(R_{sum,0}(u,v) + R_{sum,1}(u,v)\right) \left|\Delta G(u,v)\right|^2}, \tag{21}$$

and

$$SNR^2_{rate,PWMF}(f_{lmt}) = \frac{1}{T} \cdot \sum_{f \le f_{lmt}} \frac{\left|\Delta G(u,v)\right|^2}{\tfrac{1}{2} \cdot \left(R_{sum,0}(u,v) + R_{sum,1}(u,v)\right)}. \tag{22}$$

3.7 The SNR-measures obtained by integration (analytical de-biased data)

As discussed by Gagne and Wagner (1998), the direct summation over the spatial frequency channels of the estimated (biased) SNR^2 spectrum results to a biased SNR^2-value. FluoroQuality calculates also a de-biased SNR^2-estimate by their theory as

$$SNR^2_{ideal,debiased}(f_{lmt}) = \sum_{f \le f_{lmt}} SNR^2_{f,debiased}, \tag{23}$$

where

$$SNR^2_{f,debiased} = \left(\frac{2N_{eff}(f) - 3}{2N_{eff}(f) - 2} \right) \cdot \frac{\left|\Delta G(f)\right|^2}{\tfrac{1}{2} \cdot \left(R_0(f) + R_1(f)\right)} - \frac{2}{N_{eff}(f)} \tag{24}$$

is the bias-corrected SNR^2 spectrum, and $N_{eff}(f)$ is the effective number of images in either the signal or background case (see the explaining text later).

The error, σ, of $SNR^2_{ideal,\ debiased}(f_{lmt})$ is also estimated according to the theory of Gagne and Wagner (1998) by adding the variances of each included frequency channel

$$\sigma^2(SNR_f^2) = \frac{4\left(N_{eff}(f)-1\right)^3}{\left(2N_{eff}(f)-3\right)^2\left(N_{eff}(f)-2\right)}\left\{\frac{4}{N_{eff}^2(f)} + \frac{4}{N_{eff}(f)}\cdot SNR^2_{f,debiased} + \frac{\left(SNR^2_{f,debiased}\right)^2}{2(N_{eff}(f)-1)}\right\} \tag{25}$$

(The bias and variance at the spatial zero and Nyquist frequencies are actually slightly different from the expressions above: see Gagne and Wagner (1998).)

In Eqs (24–25) we have used the effective number of images, $N_{eff}(f)$, instead of the actual number of images. This is because for each imaging condition there are M files of 32 frames each used in the calculation, but the 32 frames in any of the files are not necessary statistically independent because of lag. The lag effect may depend on the spatial frequency*) and, therefore, the effective number of images at each spatial frequency is estimated separately as being

$$N_{eff}(f) = M\cdot 32\cdot\frac{R_0(f)+R_1(f)}{R_{0,sum}(f)+R_{1,sum}(f)}\ . \tag{26}$$

In FluoroQuality N_{eff} is subjected also to the condition $M \le N_{eff} \le 32\cdot M$.

The above expressions are almost similar for the calculation of the SNR^2_{rate}:

$$SNR^2_{rate,ideal,debiased}\left(f_{lmt}\right) = \frac{1}{T}\sum_{f\le f_{lmt}} SNR^2_{f,seq,debiased}\ , \tag{27}$$

where

$$SNR^2_{f,seq,debiased} = \left(\frac{2M-3}{2M-2}\right)\cdot\frac{\left|\Delta G(u,v)\right|^2}{½\cdot\left(R_{sum,0}(u,v)+R_{sum,1}(u,v)\right)} - \frac{2}{M}\ , \tag{28}$$

$$\sigma^2(SNR^2_{f,seq}) = \frac{4(M-1)^3}{(2M-3)^2(M-2)}\left\{\frac{4}{M^2} + \frac{4}{M}\cdot SNR^2_{f,seq,debiased} + \frac{\left(SNR^2_{f,seq,debiased}\right)^2}{2(M-1)}\right\} \tag{29}$$

and M denotes the number of recorded signal or background image sequences. There is no need to estimate an effective number instead of M, because the sequences can be assumed to be statistically independent.

*) Typically, the noise at low spatial frequencies is dominated by quantum noise, which is affected by the lag in the imaging system. The noise at high spatial frequencies is often dominated by temporally white electronic noise.

3.8 Temporal lag

Temporal lag was evaluated in terms of the lag factor *F* in Tapiovaara (1993). This factor compares the information rate in an image sequence to the information in a single frame and shows the effective number of independent image frames per unit time. In that paper, *F* was defined in terms of the DC-suppressing observer. Here, lag is reported in terms of quantities related to 1/*F* and the unit of the lag-measures is s.

Three slightly different measures of lag are given in the output of FluoroQuality. One is the lag measure related to the comparison of SNR^2 in a single frame and SNR^2_{rate} of the ideal observer

$$Lag_{PWMF} = \frac{SNR^2_{ideal,debiased}}{SNR^2_{rate,ideal,debiased}}. \tag{30}$$

The other one is calculated similarly to the DC/HF-suppressing observer and the third one is obtained from the DCsHFs-observer by excluding the spatial frequency axes ($u = 0$ or $v = 0$) from the summation:

$$Lag_{DCsHFs,excl.axes} = T \cdot \frac{\sum_{u\neq 0, v\neq 0} \left|\Delta G(u,v)\right|^2 \cdot \tfrac{1}{2}(R_0(u,v) + R_1(u,v))}{\sum_{u\neq 0, v\neq 0)} \left|\Delta G(u,v)\right|^2 \cdot \tfrac{1}{2}(R_{sum,0}(u,v) + R_{sum,1}(u,v))}. \tag{31}$$

This last lag measure was developed in the past, when we often experienced excessive noise on the spatial frequency axes (cross-like shape in the NPS). We have not seen these artefacts with NPS calculations made with FluoroQuality, however. Anyway, in our experience, this last lag measure is the most stable of the measures presented above, and it is used in calculating the $SNR^2_{rate,\,DCsHFs}$ as will be explained in 3.10. The error (1 STD) in the lag-measure is estimated from the expected precision of the average images and the NPS.

3.9 The DCsHFs-observer's SNR obtained using the template method

In addition to the analytical calculations explained above, FluoroQuality measures the DCsHFs-observer's SNR in the single frames by the following method: A template is calculated from the net signal $\Delta g(i, j)$ by first calculating the average pixel values of its even and odd pixel rows (these correspond to the even and odd video fields of one video frame) and subtracting

these averages from the pixel values of the respective pixel rows of the net signal. This results to a template whose DFT would have the value zero at frequencies (0, 0) and (0, v_{max})*). This template is calculated separately for each image sequence file, *m*, by leaving this sequence out in calculating the average image, and is denoted here as $\Delta g_{DCsHFs,\,m}(i,j)$. This template is then cross-correlated with each image frame in sequence *m* to get the DCsHFs-observer's conditional decision variables

$$D_{DCsHFs}(g_{k,m} \mid s) = \sum_{i,j} \Delta g_{DCsHFs,\,m}(i,j) \cdot g_s(i,j,k,m) \quad . \tag{32}$$

The SNR is then calculated from these values as shown in Eq 1.

There are also other possibilities to use the image data for the measurement. For example, one could divide the image data in two separate groups, and use one group for estimating the averages and the other for testing the performance. However, this results to inefficient use of the data and unnecessary imprecision and bias in the results. Another alternative would be not to leave out the image data being tested from estimating the average image; this would lead to biased results.

The error (1 STD) in the obtained SNR^2 is estimated as

$$\sigma\left(SNR^2_{DCsHFs}\right) = 2 \cdot SNR_{DCsHFs} \cdot \sqrt{\frac{2}{N_{eff}} + \frac{SNR^2_{DCsHFs} \cdot \left(\sigma^4(D \mid 0) + \sigma^4(D \mid 1)\right)}{2 \cdot \left(N_{eff} - 1\right) \cdot \left(\sigma^2(D \mid 0) + \sigma^2(D \mid 1)\right)^2}} \quad , \tag{33}$$

where the effective number of images is estimated from

$$N_{eff} = M \cdot \frac{T}{Lag_{DCsHFs,excl.axes}} \quad . \tag{34}$$

The SNR-measurement is subjected to a test of the equality of the variances of the decision variable *D* with the conditions of signal present and absent; the variances should be equal if the noise is truly signal-independent. The user is noted if one of the variances is more than 20% larger than the other.

The measurement is also subjected to a X^2-test of the normality of the conditional decision variables. The user is warned if the test suggests non-normality of the data (i.e., if the value of the X^2-variable is larger than the 1% significance limit).

*) To suppress only the frequency (0, 0) it is sufficient to subtract the average pixel value of the entire net signal image. However, interlaced scanning TV-systems often exhibit excessive noise also at the spatial frequency (0, v_{max}), and it is useful to suppress this frequency as well.

3.10 SNR^2_{rate}

The SNR^2_{rate} of the DCsHFs-observer is estimated in two ways: (i) by measuring the SNR^2 of the image sequences essentially as explained in 3.9, but by testing images that are averaged over the whole image sequence length (32 consecutive frames) instead of testing the individual frames as was done in 3.9; the SNR^2_{rate} is obtained by dividing the SNR^2-estimate of the averaged images by the acquisition time of the sequence, T. The other method (ii) is to estimate the SNR^2_{rate} from the SNR in single image frames and the lag as

$$SNR^2_{rate,DCsHFs} = \frac{SNR^2_{DCsHFs}}{Lag_{DCsHFs,excl.axes}} \quad . \tag{35}$$

3.11 Bias issues of SNR measurements

As already discussed in chapter 2.3, an uncorrected measurement of SNR from the average image and NPS data results to biased results, mainly because the residual noise in the averaged data will be interpreted as being part of the signal. On the other hand, the residual noise in the average images that are used in the DCsHFs-template method of SNR-measurement (Chapter 3.9) causes that the results from this method are low-biased: in this case, the noisy template does not accurately correspond to the actual signal and doesn't, therefore, perform as well as a noiseless template would do.

The SNR^2 and SNR^2_{rate} estimates from three measurement methods ((i) the analytical biased estimate, (ii) the analytical de-biased estimate and (iii) the estimate from the DCsHFs-template method) are shown in Figs 1 and 2 for 0,9–3,7 mm thick PMMA-disk signals of 1 cm diameter, obtained at different imaging conditions (varying the dose rate, the optical aperture between the image intensifier and the TV-camera, and the use of an antiscatter grid). The background phantom used in the measurements consisted of a 2 mm copper plate at the x-ray tube housing and a 4,7 cm PMMA block placed on the x-ray image intensifier. The x-ray tube voltage was 72 kV, the source-to-image distance 108 cm and the x-ray beam size at the x-ray image intensifier entrance plane 23 cm x 23 cm. The number of image files, *M*, was 40 in these measurements (i.e., 40 image sequences of 32 consecutive frames each were

recorded for both the signal and the background case). The "true" value of the SNR^2 for each disk at each separate imaging condition is obtained, by physical reasoning, as the average of the measurements by methods (ii) and (iii) above for the thickest detail at that imaging condition and scaling this SNR^2 by to the ratio of the squares of the disk thicknesses. The SNR^2-estimates are shown in Fig. 1 and the SNR^2_{rate}-estimates in Fig. 2.

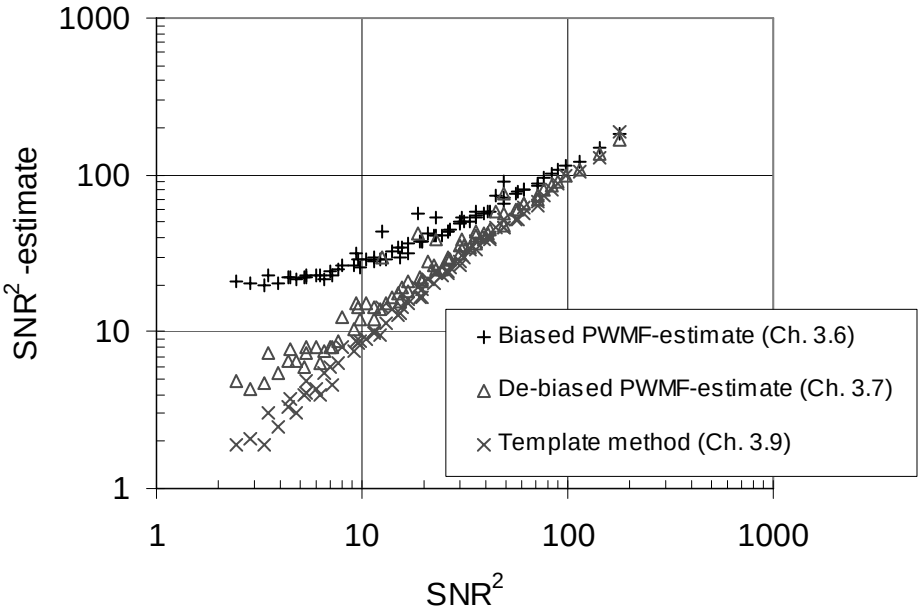

Figure 1. The estimates of the SNR^2 in single image frames as measured by three methods (Chapters 3.6, 3.7 and 3.9). The data correspond to the detectability of 1 cm diameter PMMA disks of various thicknesses in various imaging conditions. Number of signal and background image files $M = 40$. The data are plotted against the true SNR^2 of the details.

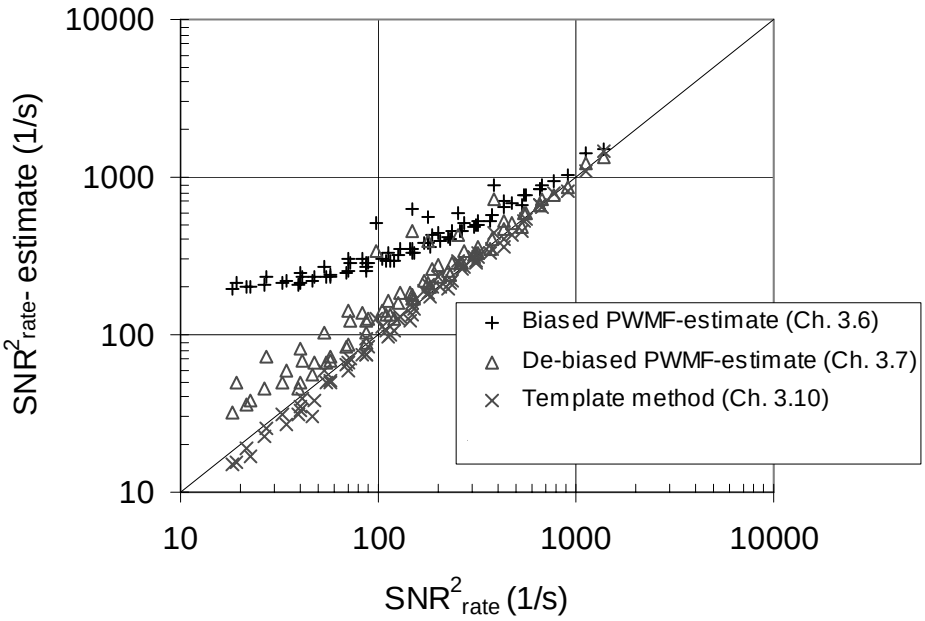

Figure 2. The estimates of the SNR^2_{rate} as measured by three methods (Chapters 3.6, 3.7 and 3.10). The data correspond to the detectability of 1 cm diameter PMMA disks of various thicknesses, in various imaging conditions. Number of signal and background image files $M = 40$. The data are plotted against the true SNR^2_{rate} of the details.

In the figures it is seen that the uncorrected (biased) SNR-estimates suffer increasingly from the bias when the SNR gets smaller; therefore, these results are not of much use. The template-method-estimates are somewhat low-biased at very low SNR's, as expected, and the de-biased SNR estimates seem to get slightly high-biased at low SNR's, in spite of the bias-correction.

The de-biased analytical SNR-data include also a few outliers, whose value is notably higher than expected. These outliers are characterised by their signal spectra including more power in their high spatial frequency region than would be expected from the actual low-frequency signal used – it seems that in some cases the averaging process of the signal and background images has not cleaned image noise in the average images as well as would be expected by the number of images. These outliers stood out also in the analytical SNR-calculation results by the strong dependence of their SNR^2-values on the maximum included frequency, $f_{lmt.}$ A possible method of reducing the bias of (truly) low-frequency signal details is then to use the SNR-estimates based on

a sufficiently low value of f_{lmt} in the analytical calculation (Gagne and Wagner 1998).

The dependence of the bias on the number of analysed image files (M) can be seen in figures 3 and 4 which represent the estimates of SNR^2 in single frames and the SNR^2_{rate} of the image sequences, respectively. The data have been measured for 1 cm diameter PMMA disk details of three thicknesses: 0 mm, 0,9 mm and 3 mm thick, (the zero thickness corresponds to no actual signal in the image: true SNR=0). The same phantom and geometry as described above was used. In the measurements the anti-scatter grid was used, the x-ray tube voltage was 72 kV and the tube current 0,7 mA.

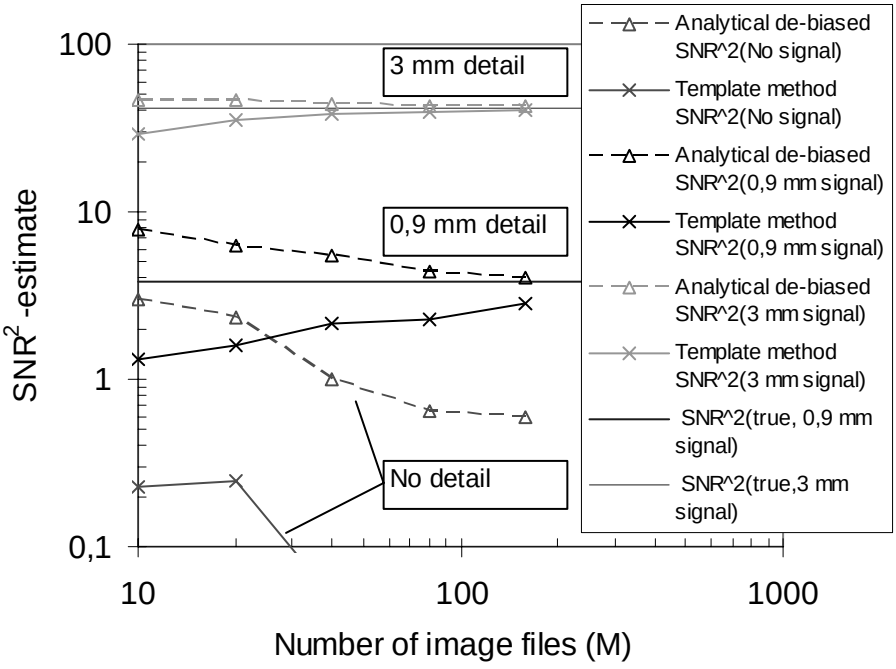

Figure 3. The SNR^2 of single image frames, estimated by two different methods for three 1 cm diameter PMMA disks of various thicknesses (0, 0,9 and 3 mm). The dashed curves correspond to analytical de-biased estimates (Chapter 3.7) and the continuous curves to the template method (Chapter 3.9). The horizontal continuous lines without data points show the expected unbiased SNR^2-value for the 3 mm and 0,9 mm detail (the latter calculated by scaling the SNR^2 of the 3 mm datum).

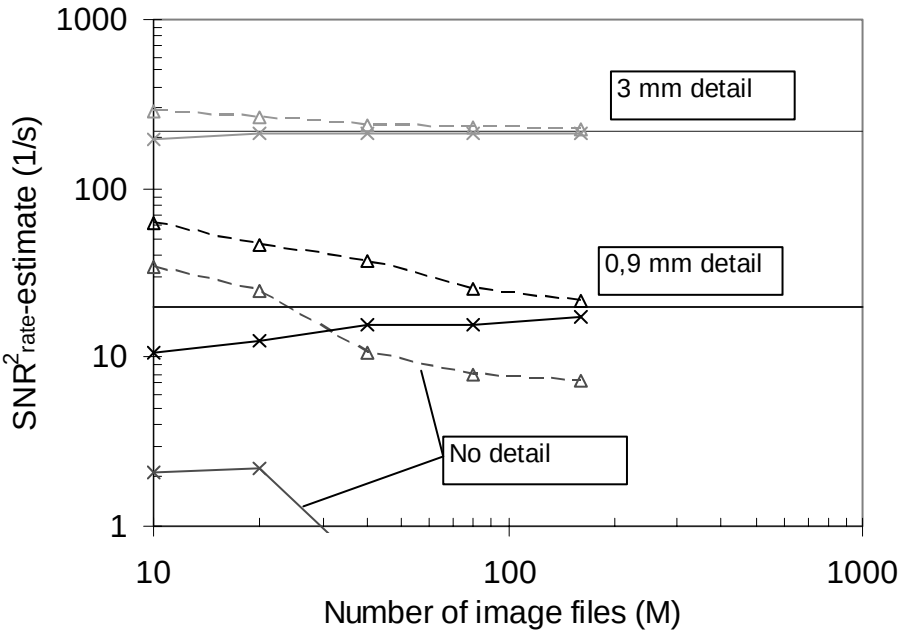

Figure 4. The SNR^2_{rate}, estimated by two different methods for three 1 cm diameter PMMA disks of various thicknesses (0, 0,9 and 3 mm). The dashed curves correspond to analytical de-biased estimates (Chapter 3.7) and the continuous curves to the template method (Chapter 3.10). The horizontal continuous lines without data points show the expected unbiased SNR^2_{rate} for the 3 mm and 0,9 mm details (the latter calculated by scaling the SNR^2_{rate} of the 3 mm datum).

For clarity of illustration, the analytical biased SNR^2 estimates have not been plotted in these figures; they were again positively biased to such a degree that they were almost useless. The bias of the analytical de-biased estimate increases slightly with a decreasing number of image files; the positive bias of this SNR^2 estimate seems to be independent of the signal strength and is of the order of 3–4 when $M = 10$. The bias of the template-based SNR^2-estimate is negative, as expected, and increases with a decreasing M. This bias is smaller for the zero and 0,9 mm details than the bias of the de-biased estimate, but larger (although small) for the 3 mm detail. The disagreement between the de-biased SNR^2 estimate and the template method SNR^2 estimate of the 0,9 mm detail is in accordance with Figure 1 and suggests that even M=160 may not be large enough to remove the bias of very faint details. One possibility to measure

the SNR^2 of such thin details might be to derive their SNR^2 from the measurement of a thicker detail by scaling with the ratio of the squares of the detail thicknesses, if possible.

Overall, the conclusions of the SNR^2_{rate} estimates are similar to those above; the bias is minor for reasonably strong signal details and an important issue only for very faint signal details. The analytical de-biased estimates are slightly positively biased, the template-method estimates are slightly negatively biased, and the bias decreases with an increasing number of image samples. In this case, however, the bias of the template-matching estimate appears to be lowest for all the details when *M* is low.

Based on the above results and our earlier experience, the DCsHFs-template-based measurement method seems to result in the most reliable SNR-estimates from the measurement alternatives considered here. The use of a low *M* and a very weak signal detail should be avoided. The bias (which is evident at low SNR^2 and SNR^2_{rate} values for moderate *M*) could perhaps be reduced by using the average of the template-based and the analytical de-biased estimates.

4 SNR^2_{rate} and detail visibility

For static radiographs, it is often said that a SNR of 3–7 (SNR^2 ~ 9–50) is needed for a detail to be visible. This is, however, just a rule of thumb trying to relate the SNR with visibility*). Actually, there is no detectability threshold, but the detail turns from not visible to clearly visible through a continuosly improving detection certainty when the SNR is increased.

The statistical efficiency $F = (d')^2 / SNR^2_{ideal}$ of humans is often found to be of the order of 50%: then, a human observer who is presented images with a detail of, say, $SNR_{ideal} = 2$ would obtain a $d' \sim 1.41$ and achieve a 84 % probability of a correct answer in a 2AFC test, or a 39 % probability in a 16-AFC test (see figure 5 for the relationship between d' and the probability of a correct response in some MAFC tests). Some authors have equated the criterion of

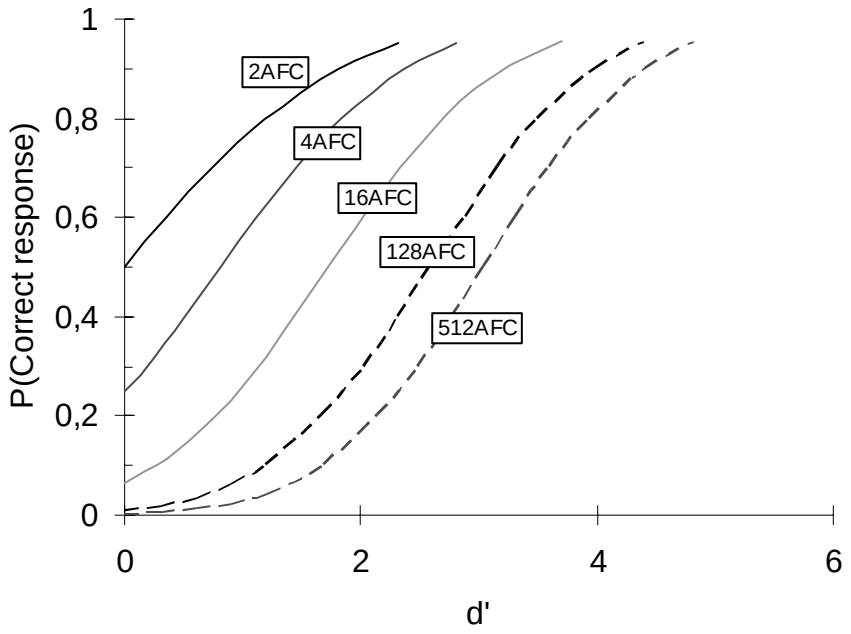

Figure 5. The relationship between the observer's signal-to-noise ratio at the decision level (*d'*) and the probability of a correct response in some MAFC tests.

*) The use of SNR thresholds has been criticized by many researchers, e.g., Burgess (1983), who also pointed out that Rose had suggested SNR threshold values (denoted by k) in the range from 3 to 5. After his criticism Burgess writes "...However if you insist on using the Rose model it is suggested that you use values of "k" in the range from 5 to 10 for simple detection and 15 to 20 for signal identification tasks".

detectability with the condition of 50 % correct responses in an 18-AFC test, which corresponds to $d' = 1{,}78$. Using the estimate of $F = 50$ %, this would correspond to the detectability of signals with SNR ≥ 2.5.

In fluoroscopy the "threshold contrast" (i.e. the lowest contrast detail that the observer subjectively judges as perceivable) is likely to depend on several factors in addition to the SNR^2_{rate}. These factors may include, e.g., the instructions given to the observers, the design of the test object, the displayed contrast, the properties of image noise, the allowed observation time and any background non-uniformity. One should also note that the inter- and intraobserver variability in visibility threshold tests is large: the "threshold" is difficult to define and keep, and may therefore have a different meaning to different observers and to a given observer at various times.

In the human observer tests that we have made, we have found an average SNR^2_{rate} for the observers declaring a detail in a noisy fluoroscopic image as just visible*) to be around 60 s^{-1}. This "threshold SNR^2_{rate}" did not seem to be independent of the noise (or dose) level, however, but increased with the dose rate (i.e., decreasing noise): the average "threshold SNR^2_{rate}" was 87 s^{-1} for a two-fold dose rate and 140 s^{-1} for a four-fold dose rate, compared to the lowest dose rate in the tests. So, the observers' visibility threshold did not improve as much as would be expected by SNR reasoning. The threshold SNR^2_{rate} variability between the observers in these tests was large, about 40%, and one should consider these "thresholds" only as typical values. Nevertheless, these figures may give a feel for the SNR^2_{rate} magnitude required for a subjective sensation of visibility.

We also made 16-AFC tests at two of the lowest dose levels referred to above. The SNR^2_{rate} of the test detail was equal to 19 s^{-1} at the lowest dose rate and equal to 40 s^{-1} at the two-fold dose rate level (i.e., the SNR^2_{rate} of the test details were about one third or one half of the SNR^2_{rate} of the details that the observers reported as just visible in the threshold-experiment). The square of the observers' mean detectability index, d'^2, was 6.6 and 12.4 in these imaging conditions, respectively. These results are compatible with the assumption that the observers' d'^2 is proportional to the SNR^2_{rate}. This suggests that in the "threshold" test the observers evaluated the detail contrast to be more important than was actually the case in the controlled detectability test.

*) The observers were instructed "to try to see through the noise but without needing to guess".

It is problematic to evaluate the statistical efficiency of the human observers in fluoroscopy because the available SNR increases with fluoroscopy time (and the efficiency would be very low), but one can think of the ratio $t_{eff} = d'^2 / SNR^2_{rate}$ as depicting the effective time that a human has integrated the information from a live image sequence. This interpretation should not be taken literally, however: the detection times in the 16AFC tests above were very long, from about 30 s to several minutes for each single observation. Anyway, the obtained result of t_{eff} å 1/3 s may be a useful rule of thumb for interpreting the meaning of SNR^2_{rate} from a human observer standpoint. This rule seems to apply even to the "SNR threshold" tests mentioned above; the "perceived SNR thresholds", $\sqrt{t_{eff} \cdot SNR^2_{rate,thresh}}$, range from 4.4 to 6.9 and are in good agreement with values quoted for static images.

It is however noted that we have earlier (Tapiovaara 1997) found a relatively high efficiency for human observers detecting static low-contrast details in dynamic noise. These earlier measurements were made using the 2AFC method and finite-length image sequences, which were replayed in a continuous loop. Interpreting the data from that study in a similar way as is done here would suggest an effective information integration time of at least 0,8 s, given that the display contrast is optimal. We do not presently know the reason for this difference between our present and earlier data, but suspect that it could be due to the much easier decision task in the 2AFC experiment compared to the 16-AFC experiment used here – having only two possible signal locations near each other does not place similar demands on memory as signal detection from several alternatives in a large image area does.

5 An example of using FluoroQuality for imaging technique optimisation

In this chapter we give an example of how FluoroQuality can be used for optimising the imaging technique for a given detection task*). This example is related to interventional imaging, and considers the detectability of an USCI 5F catheter (type 08LF0878) in an about 25 cm thick patient. The measurement is easy and quick; the measurements described here were made in less than two hours.

The patient-simulating phantom consisted of several slabs, whose total thicknesses were 20.5 cm polymethyl methacrylate (PMMA), 4.3 mm aluminium and 5 mm water; the lateral extent of the phantom was 24 cm x 24 cm. A 13 mm piece of the catheter was filled with water and immersed in the water layer on top of the phantom, in order to mimic its contrast within a vein (in this case without any contrast material). The distance between the x-ray tube focal spot and the image intensifier entrance plane was 110 cm, and the field size at the image intensifier entrance plane was 20 cm x 20 cm. The distance between the x-ray tube focal spot and phantom top was 87 cm.

The x-ray equipment used for the measurements consisted of a Valmet BR 2001 three-phase 12-pulse high-voltage generator, a rotating anode x-ray tube (Comet DI 10 HS 22/52-150, total filtration without any added filter 2.1 mm Al), a Philips Imagica 23 cm image intensifier and an XTV-11 video chain with a low-lag Vidicon (Newvicon) pick-up tube operated in the 625 lines/ frame interlaced scan mode. A stationary antiscatter grid (strip density 44 line pairs cm^{-1}, grid ratio 10:1, carbon fibre cover plates, focusing distance 1 m) was located in front of the image intensifier entrance plane.

The phantom was imaged in the fluoroscopic mode, using various imaging conditions (with and without an added 0.25 mm Cu-filter, several x-ray tube voltages). The x-ray tube voltage and current were chosen manually but the gain in the video chain was automatically controlled. The fluoroscopic sequences were recorded both with and without the signal detail (13 mm piece of the USCI 5F catheter) in the analysed image area by using a Matrox Genesis LC frame grabber board and the NoiseAcquisition-program (see Appendix A). The image sequences were analysed with the FluoroQuality-program. The

*) The optimum imaging conditions are defined as those that result to the lowest dose in the patient for a specified image quality.

entrance air kerma rates (EAK, free-in-air) were measured using a Radcal 9015 dosemeter equipped with a 10x5-6 ionisation chamber. The x-ray tube voltage was monitored using a Machlett Dynalyzer II voltage divider chain. Figure 6 shows the average images and a sample image frame in one of the imaging conditions.

(a) (b) (c)

Figure 6. An example of the images in the detection task. (a) The average image for the signal; the catheter located in the phantom. (b) The average image for the background; the catheter removed from the phantom. (c) A one-frame sample from the image series with the catheter in the phantom. 65 kV, 5.7 mA, filtration 2.1 mm Al + 0.25 mm Cu, EAK 3.93 mGymin^{-1}, SNR^2_{rate} 891 s^{-1}, SNR of single frames 10.7.

Table 1 shows the measured imaging conditions together with the measurement results of SNR^2_{rate} and dose rate. (Note that the data have not been acquired by using the automatic dose rate control, and the dose rate does not, therefore, decrease with an increasing tube voltage. This does not affect our analysis here, because the system is well quantum noise limited; this can be seen, e.g., from the data at 2.1 mm Al filtration, 65 kV; 0.3 and 2.1 mA.) The rate of the effective dose was calculated with the PCXMC -program (Tapiovaara et al. 1997). The effective dose data given in Table 1 correspond to the PA-projection in a cardiological procedure of an obese patient (174 cm height and 105 kg mass).

Figures 7 and 8 show the dose-to-information conversion factors (SNR^2_{rate}/dose rate) calculated from the data and corresponding to the air kerma rate and the rate of effective dose, respectively. The data have been plotted as a function of the x-ray tube voltage for both filter choices.

Table I. Measurement data for the optimisation example of detecting a catheter in the heart of a 25 cm thick patient. SNR^2_{rate} is calculated as the average of two estimates (Chapters 3.7 and 3.10)

Total filtration	kV	mA	Air kerma rate (mGy/min)	Effective dose rate (σSv/min)	SNR^2_{rate} (1/s)
2.1 mmAl	45	6.3	11.0	86.5	574
2.1 mmAl	50	2.5	5.75	56.2	417
2.1 mmAl	55	1.0	2.84	33.2	273
2.1 mmAl	60	0.5	1.70	23.2	165
2.1 mmAl	65	0.3	1.18	18.3	121
2.1 mmAl	65	2.1	8.55	133	792
2.1 mmAl	70	1.1	5.15	90.0	466
2.1 mmAl	75	0.7	3.68	71.8	331
2.1 mmAl	80	0.5	2.90	62.6	260
2.1 mmAl	85	0.5	3.22	76.1	249
2.1 mmAl	90	0.5	3.55	91.0	280
2.1 mmAl	95	0.5	3.90	107	290
2.1mmAl+0.25 mmCu	50	6.3	1.42	31.8	310
2.1mmAl+0.25 mmCu	55	6.3	2.22	58.8	531
2.1mmAl+0.25 mmCu	60	6.3	3.20	97.3	747
2.1mmAl+0.25 mmCu	65	5.7	3.93	134	891
2.1mmAl+0.25 mmCu	70	3.7	3.36	126	693
2.1mmAl+0.25 mmCu	75	2.3	2.61	107	505
2.1mmAl+0.25 mmCu	80	1.5	2.09	92.4	350
2.1mmAl+0.25 mmCu	85	1.1	1.84	86.5	305
2.1mmAl+0.25 mmCu	90	0.8	1.56	77.2	209
2.1mmAl+0.25 mmCu	95	0.6	1.39	71.8	176

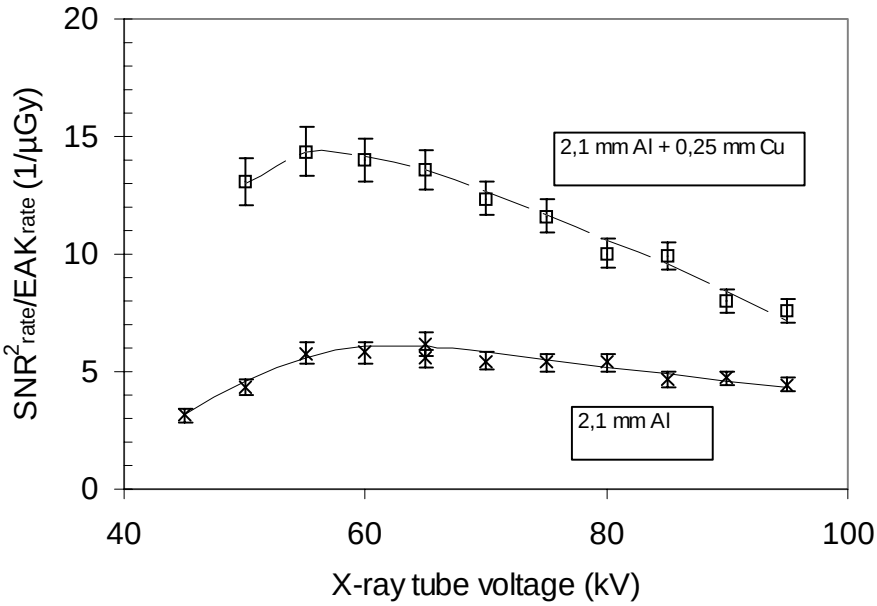

Figure 7. The dose-to-information conversion coefficient for detecting a 13 mm long piece of the USCI 5F catheter in a 25 cm thick patient. In this figure, the entrance air kerma rate (free-in-air) is used. x: total filtration 2.1 mm Al, □: total filtration 2.1 mm Al + 0.25 mm Cu, curves fitted by hand.

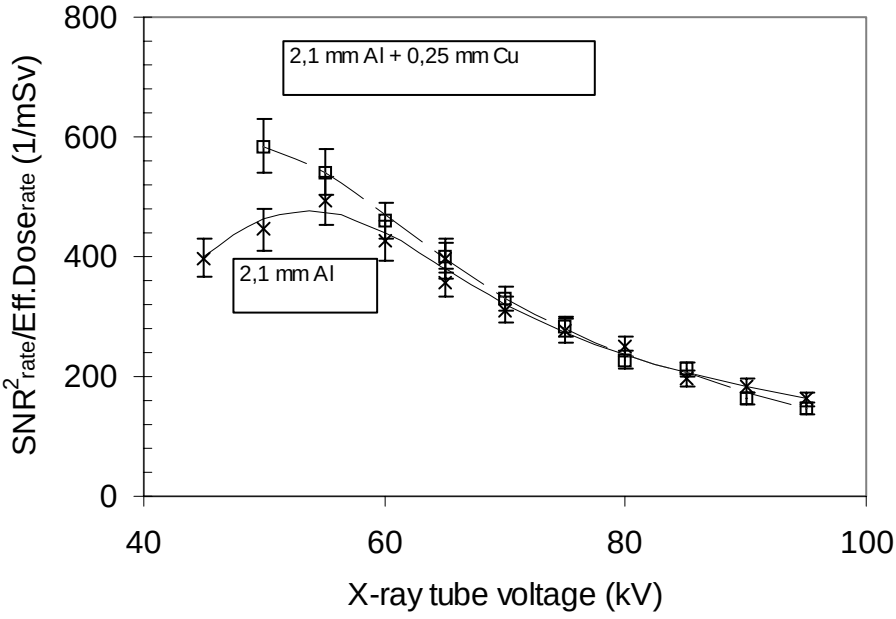

Figure 8. The dose-to-information conversion coefficient for detecting a 13 mm long piece of the USCI 5F catheter in a 25 cm thick patient. In this figure, the rate of effective dose is used and the x-ray projection is heart PA (see text for details). x: total filtration 2.1 mm Al, □: total filtration 2.1 mm Al + 0.25 mm Cu, curves fitted by hand.

From the data in figure 7 it is seen that filtration has a large effect on the entrance dose-based imaging efficiency, whereas the curves are relatively flat as a function of the tube voltage. If the skin dose of the patient is of importance (as it may be in lengthy interventional procedures) it is then best to use a highly filtered x-ray beam and an x-ray tube voltage between 50 and 70 kV (the optimum is at 55 kV). At these conditions the entrance dose rate is lowest for the given detectability of the catheter.

If the skin dose cannot be high enough to cause deterministic radiation effects in the skin, it is more reasonable to optimise the imaging conditions by using the effective dose, as has been done in figure 8. Again, the optimum among the tested alternatives is achieved by using the additional copper filter, but now the optimum x-ray tube voltage is even lower than it was when the optimum was based on the entrance air kerma rate. The effect of filtration on the dose-to-information conversion coefficient is much weaker for the effective dose rate-based evaluation than it is for the entrance air kerma rate-case. Not much advantage is gained by adding filtration – in fact, the imaging efficiency of the more heavily filtered radiation appears to be lower than for the lightly filtered radiation when the tube voltage is high. The imaging efficiency is seen to depend strongly on the x-ray tube voltage; the dose rate required for a constant detectability of the catheter is much higher at a high x-ray tube voltage than it is at voltages near 50 kV.

The above discussion considers only the imaging efficiency (SNR^2_{rate}/dose rate). For an actual optimisation of imaging conditions one needs also to specify the image quality that is required in the clinical procedure and take into account the constraints imposed by the x-ray system. For minimising the dose, it may be even more important to keep the image quality as low as is sufficient than to work at the exactly optimum imaging efficiency conditions (of course, however, the quality must be high enough to ensure the proper performing of the examination or procedure).

If good-quality imaging is necessary, the thermal load of the x-ray tube may become too high at the technique using heavy filtration and a low tube voltage, or the fluoroscopic current may be limited such that the required image quality cannot be achieved at these imaging conditions. Then, one must use less filtration or a higher tube voltage than the optimum efficiency conditions would suggest.

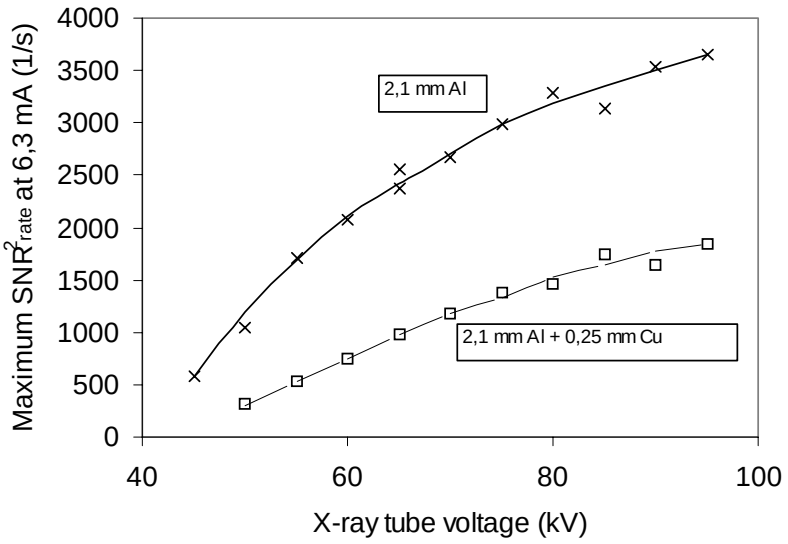

Figure 9. The SNR^2_{rate} that could be expected at a tube current of 6,3 mA (the maximum for the x-ray equipment used in the measurement), as based on the data in Table and the quantum noise limited behaviour of the imaging system. x: total filtration 2.1 mm Al, □: total filtration 2.1 mm Al + 0.25 mm Cu, curves fitted by hand.

Figure 9 shows an estimate of the maximum SNR^2_{rate} in our x-ray system at each tube voltage and filtration (the maximum tube current in our x-ray system is 6.3 mA). The estimate is based on the data in Table and assumes that our imaging chain is quantum noise limited. Now, if the required image quality would correspond to an SNR^2_{rate} of 1500/s, for example*), it would be better to image the patient without the copper filter, because the copper filter would require a tube voltage of at least 80 kV in order to achieve the required image quality. The efficiency is low at such high voltages, and the aluminium-filtered system operating at 55 kV would in this case allow an about 50% lower effective dose rate (see fig. 8). The actual optimum condition of this example would require a filtration between the two examples here**): the optimum filter would be the thickest filter that allows the use of an x-ray tube voltage near 50–55 kV. If we could use a higher power x-ray system the optimum filter thickness would be larger.

*) This would be a high quality fluoroscopic image: roughly, discarding effects of resolution, even the SNR^2_{rate} for a 1 mm piece of the catheter would be equal to about 1500/13 = 115, which suggests easy detectability of catheter details of such size.

**) The lower filtration in this example is below the minimum allowed filtration of medical x-ray equipment. The use of such filters is not suggested: a system working between the two filter examples considered would be the optimal choice here.

6 Acknowledgements

This work was partly funded by the European Commission's 5th Framework Programme (1998–2002), Nuclear fission and Radiation Protection Contract, DIMOND III (FIGM-CT-2000-00061). This report is the sole responsibility of the author and does not reflect the opinion of the European Commission or STUK. The European Commission or STUK are not responsible for any use that might be made of data appearing in this report.

7 References and further reading

Barrett HH and Swindell W, *Radiological Imaging, Volumes I and II*, Academic Press, New York, 1981.

Barrett HH and Myers K, *Foundations of Image Science: Mathematical & Statistical Foundations,* John Wiley and Sons, to be published 2003.

Beutel J, Kundel H, Van Metter R (eds.), *Handbook of Medical Imaging, Vol 1: Me*dical Physics and Psychophysics, SPIE, Bellingham 2000.

Bochud FO, Valley J-F, Verdun FR, Hessler C and Schnyder P, Estimation of the noisy component of anatomical backgrounds, Med.Phys. 26, 1365–1370, 1999.

Brown DG, Insana MF and Tapiovaara M, Detection performance of the ideal decision function and its McLaurin expansion: Signal position unknown, J.Acoust.Soc.Am. 97, 379–398, 1995.

Burgess AE, Observer performance testing for medical imaging, Notes for A.A.P.M. refresher course – August 1983.

Burgess AE, Comparison of receiver operating characteristic and forced choice observer performance methods, Med.Phys. 22, 643–655, 1995.

Burgess AE, Wagner RF, Jennings RJ and Barlow HB, Efficiency of human visual signal discrimination, Science 214, 93–94, 1981.

Burgess AE, Jacobson FL and Judy PF, Lesion detection in digital mammograms, Proc.SPIE 4320, 555–560, 2001a.

Burgess AE, Jacobson FL and Judy PF, Human observer detection experiments with mammograms and power-law noise, Med.Phys. 28, 419–437, 2001b.

Cahn RN, Cederström B, Danielsson M, Hall A, Lundqvist M, Nygren D, Detective quantum efficiency dependence on x-ray energy weighting in mammography, Med.Phys. 26, 2680–2683, 1999.

Chakraborty DP, Physical measures of image quality in mammography, Proc. SPIE 2708, 179–185, 1996.

Chakraborty DP, Computer analysis of mammography phantom images (CAMPI): An application to the measurement of microcalcification image quality of directly acquired digital images, Med.Phys. 24, 1269–1277, 1997a.

Chakraborty DP, Comparison of computer analysis of mammography phantom images (CAMPI) with perceived image quality of phantom targets in the ACR phantom, Proc. SPIE 3036, 160–167, 1997b.

Chakraborty DP, Sivarudrappa M and Roehrig H, Computerized measurement of mammographic display image quality, Proc. SPIE 3659, 131–141, 1999a.

Chakraborty DP, Effect of antiscatter grid and target/filters in full-field digital mammography, Proc. SPIE 3659, 878–885, 1999b.

Cunningham IA, Moschandreou T, Subotic V, Detective quantum efficiency of fluoroscopic systems: the case for a spatial-temporal approach (or, does the ideal observer have infinite patience?), Proc. SPIE 4320, 479–488, 2001.

Dainty JC and Shaw R, *Image Science*, Academic Press. London, 1974.

Dobbins JT III, Effects of undersampling on the proper interpretation of modulation transfer function, noise power spectra, and noise equivalent quanta of digital imaging systems, Med.Phys. 22, 171–181, 1995.

Dobbins JT III, Ergun DL, Rutz L, Hinshaw DA, Blume H and Clark DC, DQE(f) of four generations of computed radiography acquisition devices, Med.Phys. 22 1581–1593, 1995.

Fujita H, Ueda K, Morishita J, Fujikawa T,Ohtsuka A and Sai T, Basic imaging properties of a computed radiographic system with photostimulable phosphors, Med.Phys. 16, 52–59, 1989.

Fukunaga K, *Introduction to Statistical Pattern Recognition*, Academic Press, New York 1972.

Gagne RM and Wagner RF, Prewhitening matched filter: practical implementation, SNR estimation and bias reduction, Proc. SPIE 3336, 231–242, 1998.

Gagne RM, Myers KJ and Quinn PW, Effect of shift invariance and stationarity assumptions on simple detection tasks: spatial and spatial frequency domains, Proc. SPIE 4320, 373–380, 2001a.

Gagne RM, Boswell JS, Myers KJ and Peter G, Lesion detectability in digital radiography, Proc. SPIE 4320, 316–325, 2001b.

Goldman LW, Fluoroscopic performance tests using a portable computer/frame grabber: Wiener spectra measurements, Med. Phys. 20, 117–127, 1992.

Green DM and Swets JA, *Signal Detection Theory and Psychophysics*, John Wiley and Sons, New York, 1966.

Hanson KM, Variations in task and the ideal observer, Proc. SPIE 419, 60–67, 1983.

ICRU Report 41, Modulation Transfer Function of Screen-Film Systems, International Commission on Radiation Units and Measurements, 1986.

ICRU Report 54, Medical imaging – the assessment of image quality, International Commission on Radiation Units and Measurements, 1996.

Kotre CJ, The effect of background structure on the detection of low contrast objects in mammography, Br. J. Radiol. 71,1162–1167, 1998.

Loo L-ND, Doi K, and Metz CE, A comparison of physical image quality indices and observer performance in the radiographic detection of nylon beads, Phys.Med.Biol. 29, 837–856, 1984.

Marshall NW, The practical application of signal detection theory to image quality assessment in x-ray image intensifier-TV fluoroscopy, Phys.Med.Biol. 46, 1631–1649, 2001.

Marshall NW, Kotre CJ, Robson KJ and Lecomber AR, Receptor dose in digital fluorography: a comparison between theory and practice, Phys.Med.Biol. 46, 1283–1296, 2001.

Martin CJ, Sharp PF and Sutton DG, Measurement of image quality in diagnostic radiology, Applied Radiation and Isotopes 50, 21–38, 1999.

Metz CE, Wagner RF, Doi K, Brown DG, Nishikawa RM, Myers KJ, Toward consensus on quantitative assessment of medical imaging systems, Med. Phys. 22, 1057–1061, 1995.

Moy JP, Signal-to-noise ratio and spatial resolution in x-ray electronic imagers: is the MTF a relevant parameter?, Med.Phys. 27, 86–93, 2000.

Myers KJ and Barrett HH, Addition of a channel mechanism to the ideal-observer model, J.Opt.Soc.Am.A 4, 2447–2457, 1987.

Myers KJ, Rolland JP, Barrett HH and Wagner RF, Aperture optimization for emission imaging: effect of a spatially varying background, J.Opt.Soc.Am.A 7,1279–1293, 1990.

Pineda AR and Barrett HH, What does DQE say about lesion detectability in digital radiography?, Proc. SPIE 4320, 561–569, 2001.

Siewerdsen JH, Antonuk LE, El-Mohri Y, Huang W and Cunningham IA, Signal, noise power spectrum, and detective quantum efficiency of indirect-detection flat-panel imagers for diagnostic radiology, Med.Phys. 25, 614–628, 1998.

Siewerdsen JH, Cunningham IA and Jaffray DA, A framework for noise-power spectrum analysis of multidimensional images, Med. Phys. 29, 2655–2671, 2002.

Smith WE and Barrett HH, Hotelling trace criterion as a figure of merit for the optimization of imaging systems, J.Opt. Soc.Am.A 3, 717–725, 1986.

Tapiovaara MJ, SNR and noise measurements for medical imaging: II. Application to fluoroscopic x-ray equipment, Phys.Med.Biol. 38, 1761–1788, 1993.

Tapiovaara MJ, Efficiency of low-contrast detail detectability in fluoroscopic imaging, Med.Phys. 24, 655–664, 1997.

Tapiovaara MJ and Wagner RF, SNR and DQE analysis of broad spectrum x-ray imaging, Phys. Med.Biol. 30, 519–529, 1985 (Corrigendum : Phys.Med.Biol. 31, 195).

Tapiovaara MJ and Wagner RF, SNR and noise measurements for medical imaging: I. A practical approach based on statistical decision theory, Phys.Med.Biol. 38, 71–92, 1993.

Tapiovaara MJ, Lakkisto M and Servomaa A, PCXMC – A PC-based Monte Carlo program for calculating patient doses in medical x-ray examinations, Report STUK-A139, 1997.

Tapiovaara MJ, Sandborg M and Dance DR, A search for improved technique factors in paediatric fluoroscopy, Phys.Med.Biol. 44, 537–559, 1999.

Tapiovaara MJ, Servomaa A, Sandborg M and Dance DR, Optimising the imaging conditions in paediatric fluoroscopy, Rad.Prot.Dosim. 90, 211–216, 2000.

van Trees HL, *Detection, Estimation, and Modulation Theory*, John Wiley and Sons, New York 1968.

Wagner RF, Low-contrast sensitivity of radiologic, CT, nuclear medicine, and ultrasound medical imaging systems, IEEE Transactions on Medical Imaging MI-2, 105–121, 1983.

Wagner RF, Characteristic images emerging from recent SPIE medical image symposia, Proc. SPIE 767, 138–141, 1987.

Wagner RF and Brown DG, Unified SNR analysis of medical imaging systems, Phys.Med.Biol. 30, 489–518, 1985.

Wagner RF, Beiden SV and Campbell G, Multiple-reader studies, digital mammography, computer-aided diagnosis – and the Holy Grail of imaging physics (I), Proc. SPIE 4320, 611–618, 2001.

Whalen AD, *Detection of Signals in Noise*, Academic Press, New York, 1971.

APPENDIX A: FLUOROQUALITY (V. 2.0) USER'S GUIDE

General

FluoroQuality can be used for the measurement of the quality of fluoroscopic image sequences. These sequences need first be recorded digitally by a PC/ frame grabber system using suitable software, or reformatted from the digitally stored image sequence data of the x-ray imaging system*). The FluoroQuality program then calculates and displays the SNR of single image frames, the SNR^2_{rate} of the acquired image sequences, the lag, and the spatio-temporal NPS for the acquired image data. The program also displays the average image for the signal and background situations, the net signal, the SNR^2- and SNR^2_{rate} -spectra, and can be used for visualising the acquired image data.

The signal detail need not be located in a homogeneous phantom – in principle, also an anatomic phantom may be used. However, strong background structures in the phantom may violate the assumption of noise stationarity and therefore make the NPS-measurements uncertain. Strong phantom structures may also make the detectability of the signal detail highly dependent on the actual location of the detail in the phantom, and therefore achieving a good repeatability of SNR-results may be difficult. Therefore, we recommend using a homogeneous phantom for most measurement applications. For typical applications, the signal detail should be strong enough for obtaining accurate results (see Ch. 3.11), but its contrast should be not too high in order to make the noise too much signal-dependent or the SNR-results dependent on the linearity of the imaging system and frame grabber.

The present version (FluoroQuality 2.0) is compatible with the image data acquired using the program "Filetall" (developed in STUK for the Data Translation DT3852 frame grabber card) or "NoiseAcquisition" (developed by Olander and Sandborg in Linköping University Hospital for the Matrox Genesis-LC frame grabber board). These programs require the user to define a six-character name for the data. In this manual this name is denoted as "xyzxyz".

*) Requirements for the data are given in Appendix D.

Hardware and software requirements

FluoroQuality runs under 32-bit Windows operating systems (Windows 95/98/NT/2000/XP). The memory requirement depends on the operating system, but is 64 MB RAM for a PC operated under Windows NT4 (we suggest however a minimum of 128 MB). The PC also needs sufficient hard disk space to store the image data (about 10,3 MB for each measurement comprising of 40 background and 40 signal datafiles) and the analysed data (1,37 MB for each measurement) that the user wishes to keep.

In order to keep the computation times reasonably short, one should use a fast PC. 233 MHz is a suggested minimum clock frequency.

Installation of the program

The program is installed by running the setup.exe -program of the FluoroQuality Installation Diskette. The program can be installed in any folder[*)]. The setup program creates also a subfolder "\AnalysedData" which is used for saving the data that the program calculates. Also a subfolder "\ImageData" is created; it is intended to be the folder where the image data are saved by the acquisition program. When the analysing calculation is started, the program first tries to look for image data in the folder "\ImageData", if such a folder exists. If not, the file open-dialog window is set to the program-containing folder and the user locates the data him/herself.

The setup -program will add a shortcut to the FluoroQuality in the "Programs" -menu. For an even more easy access to the program, you may create a shortcut to the FluoroQuality20.exe-file on your desktop.

---

*) If used with the above mentioned image data acquisition programs, the FluoroQuality20.exe-file is most conveniently installed in the folder 'X:\Koe'. In this case it is handy to delete the subfolder '\ImageData': then the data search will begin directly in the data folder used by these acquisition programs (X:\Koe).

Using the program

Buttons

When started, the program displays the Analysis-form (below). The form has nine buttons and other functions.

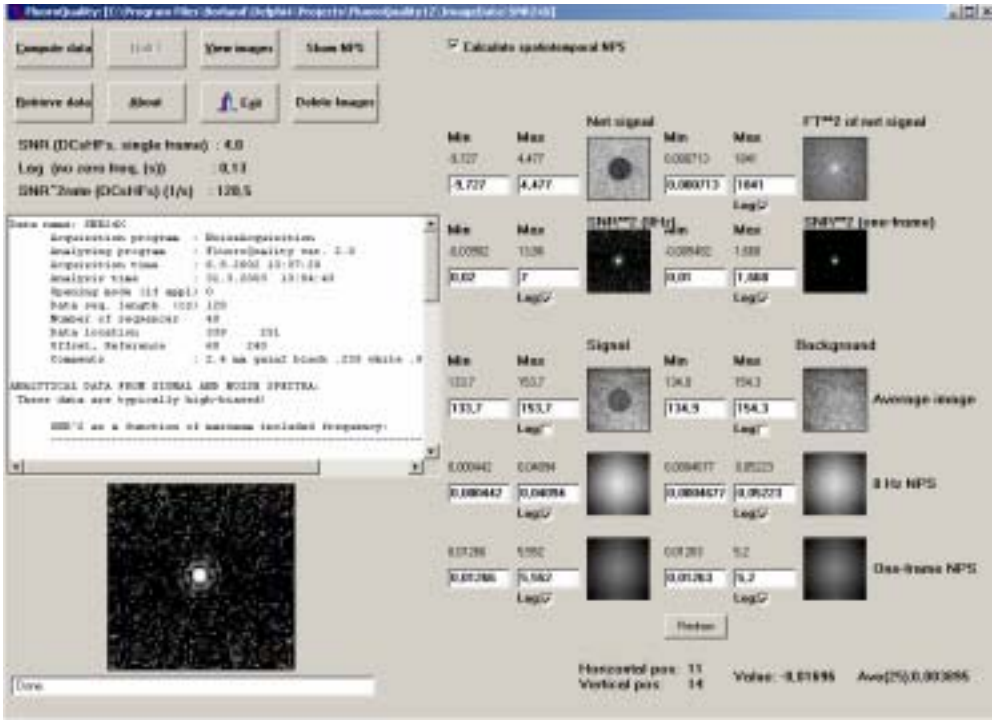

• The **Compute data** -button is used for analysing the image data (computation of results). When clicked, an open-dialog window is shown, where the user may choose one or several image data series (indicated by their parameter-file name xyzxyzPM.dat. Several files can be chosen by using the Ctrl- or Shift-keys). When clicked OK, the program calculates the analysis data for all of the chosen image series. If the **Calculate spatiotemporal NPS** -checkbox is checked, the program calculates these data as well. Calculating spatio-temporal NPS data is not necessary if the user is only interested in SNR measurements.

The SNR calculation is not performed if the data have already been analysed; i.e., if the AnalysedData-folder already contains the file xyzxyz.txt (the summary file of SNR-data). The NPS-calculation is not done if the AnalysedData folder already contains the files xyzxyzbg.spt and xyzxyzsg.spt (the spatio-temporal NPS for the background and signal image series, respectively) or if the NPS-calculation check-box is unchecked.

The calculation can be stopped by clicking the **Halt** -button at any time when the button is enabled. The remaining data can be analysed later by choosing the same set of PM-files for computation.

• The **Retrieve data** -button is used for examining data that have already been analysed. When clicked, an open-dialog window is shown, where the user can choose one of the data sets that have been analysed earlier (files indicated by their analysed data file name xyzxyz.txt). The images in the Analysis-form will be updated and the xyzxyz.txt file is shown in the memo-window.

• The **View images** -button can be used for viewing the original image data series (if they haven't been deleted from the computer). The data can be viewed either as individual frames or as a continuous loop with an user-specified frame refresh interval (specified in milliseconds). The average signal image or background image can be subtracted from the images, which may, for example, help in recognising jitter or background-structure problems in the image data. Note that any image series can be chosen for viewing. However, the subtracted average is always from the image set identified in the caption of the form.

• The **Show NPS** -button is used for displaying the spatio-temporal NPS data. It is explained in more detail in the next chapter.

• The **Delete images**-button is an easy way to delete original raw-image data when they are not needed anymore; if the data have been analysed and there is no reason to directly view the images. When this button is clicked an open-dialog window is shown, where the user can choose one or several data sets that are wished to be deleted (files indicated by their parameter file name

xyzxyzpm.dat). The file xyzxyzPM.dat and the image files xyzxyzYY.ims and xyzxyzYY.imt will be deleted (YY ranges from 01 to the actual number of image files).

- The **Redraw**-button redraws the images on the Analysis form. (A part of the images may occasionally become white because other windows (e.g. OpenDialog) may destoy their contents. The images are not automatically updated, but clicking this button restores them.)
- The **About**-button shows information of the program.
- The **Exit**-button is used for closing the program.

Other functional features of the analysis form

- On the left of each image on the form are shown the minimum and maximum values of the image data. The edit-boxes show the displayed level of black and white (with other grey values in between). The brightness and contrast of the images can be adjusted by changing the values in the edit-boxes. The displayed image is updated immediately when a change in the edit-box is made.
- Checking the Log-boxes result in displaying the image data as the logarithm of the actual value – this may help in studying images with a large data range. The black level is set at the logarithm of the value in the Min-edit-box and the white level at the logarithm of the Max-edit-box. The displayed image is updated immediately when a change in the Log-box is made.
- When the cursor is moved on an image, the position of the cursor and the actual image value (not the displayed grey level) is shown at the bottom of the form. In addition to this, the average of data in a 5x5 pixel ROI (region of interest) centered on the chosen pixel is displayed. This average is denoted by 'Ave(25)'.

Note that for the average images and the net image the position data show the coordinates of the pixel in the image; in the Fourier transform images (NPS, FT^2 of the net signal, SNR^2-spectra) the position data relates to the spatial frequency component, and the $f_x = 0$, $f_y = 0$ frequency is located at the centre of the image.

Spatial frequencies are expressed as integers. The values of horizontal and vertical frequencies in units of mm^{-1} can be obtained by dividing the displayed frequency value by the width or height of the analysed image area (in mm), respectively.

- Clicking inside an image results to a zoomed copy of that image in the lower left image box.

- Double-clicking in the Memo results to a copy of the memo text to be copied on the Clipboard.
- The SNR, SNR^2_{rate} and lag (measured by the template method) are indicated on the left side of the basic form, above the memo.

Contents of the images on the analysis-form

The contents of the image data are explained by their labels. The displayed images are:

- The sample averages of all signal and background images in terms of pixel values.
- The temporal 0-frequency NPS of the signal and background image sets. The values are in terms of pixel values and the normalisation does not include the spatial and temporal extent of the images. Nominally, a 1 mm^2 area and 1 s duration is assumed: to normalise properly to units of mm^2s, the data should be multiplied by the area of the images (in mm^2) and the temporal length (in s).
- The one-frame NPS (i.e. spatio-temporal NPS summed over all temporal frequencies) of the signal and background image sets. The values are in terms of pixel values and the normalisation does not include the spatial extent of the images. Nominally, a 1 mm^2 area is assumed: to normalise properly to units of mm^2, the data should be multiplied by the area of the images (in mm^2).
- The net signal: average signal image minus average background image.
- The square of the FFT of the net signal.
- The spectrum of the ideal observer's (prewhitening matched filter) SNR^2 for the one-frame and temporal zero-frequency cases. The display is for the de-biased estimate, unless otherwise indicated by a blue text 'Biased SNR-data' under the images. This happens if the files containing the SNR^2 spectra have been deleted.
- The text in the memo is identical to the file \AnalysedData\xyzxyz.txt and displays summary information mainly on SNR-measurements.

Show NPS-button

The **Show NPS**-button is used for displaying the spatio-temporal NPS spectra of the signal and background image set. The form used for NPS display is shown below.

The minimum and maximum value of the data set is shown in the upper left corner. The brightness and contrast of the NPS images can be set by modifying the Min- and Max-edit-boxes: these values set the levels of black and

white, intermediate grey-levels are used for the values between Min and Max. Checking the Log-box results in displaying the logarithm of the NPS-values: this helps in providing a wider dynamic range for the display. In the NPS-form, modifying the values in the Min- or Max- editboxes or checking the log-box does not result in immediate display of the NPS: in order to display the data, the user must click the **Draw**-button.

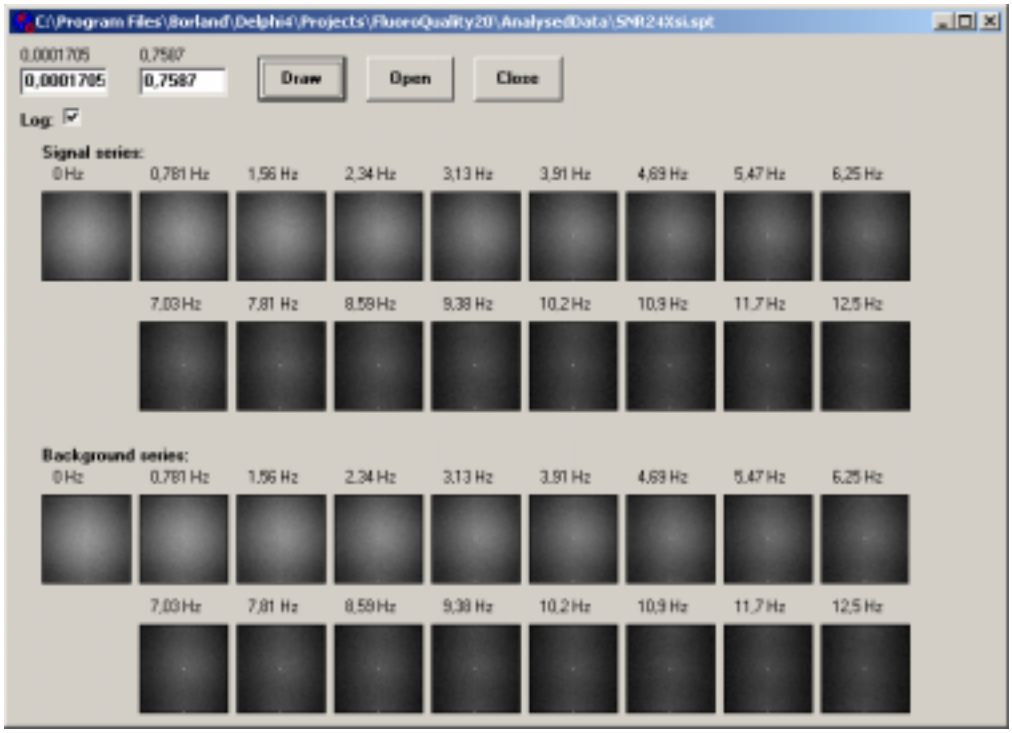

The spatio-temporal NPS values are in terms of pixel values and the normalisation does not include the spatial and temporal extent of the images. Nominally, a 1 mm^2 area and 1 s duration is assumed: to normalize properly to units of mm^2s, the data should be multiplied by the area of the images (in mm^2) and the sequence's temporal length (in s) .

The temporal frequency shown above the spectra is calculated as based on the image duration datum that is given in xyzxyzPM.dat.

The NPS of any image data can be displayed: the data name is shown in the form caption. Use the **Open**-button.

The NPS-form is closed and the basic form displayed by clicking the **Close**-button.

APPENDIX B: INTERPRETATION OF THE DATA IN XYZXYZ.TXT

The file first contains identification information: Data name and details of the acquisition of the image data.

The next section is a summary of the analytical calculations from the average image and NPS measurements in the basic form. The biased SNR estimates are calculated for the DCsHFs-observer and the PWMF (ideal) observer*) and the de-biased estimate for the PWMF-observer. The table shows the results as a function of included frequency channels: all frequencies, the frequencies below $30 \cdot f_{min}$, below $15 \cdot f_{min}$ and below $7 \cdot f_{min}$ included. Here, f_{min} is the spatial frequency resolution in the measurement: $f_{min} = 1/X$, and X is the spatial extent (width or length) of the image area analyzed.

The lag factors have been calculated analytically from the average images and the NPS data. Here, they are reported in units of a second, and are the reciprocals of the lag factors specified in Tapiovaara (1993), where the lag factor was defined as the number of statistically independent frames in a second.

The direct SNR measurement section contains the SNR data that are obtained by employing the DCsHFs-observer. The SNR^2_{rate} data have been obtained by two ways. The first figure is the SNR^2 of a single frame divided by the lag from the analytical calculation (spatial frequency 0-axes excluded from the calculation). The second is the result from direct measurement using the averaged sequence data. The latter might be preferred by being more direct, but may suffer from the small number of image data ($M+M$). Therefore, we prefer using the first SNR^2_{rate}-measure.

The user is warned if the variance of the DCsHFs-observers decision variable differ by more than 20% in the signal included and signal absent cases. In principle, the variances should be equal.

The $SNR_{single\ frame}$ measurement has an extra check for the normality of the decision variable: the chi^2-test. There is a warning if the data are not compatible with the underlying assumption of the decision variable values being normally distributed. If this warning is seen and the value is suspiciously high, there is probably a problem in the acquired data, or other than pure noise processes in the fluoroscopy system.

*) These first two SNR-estimates are usually high-biased and should not be used as such for evaluating detail detectability.

APPENDIX C: WHICH FILES ARE NECESSARY TO KEEP AND THE CONTENTS OF THE DATAFILES

• If disk space need to be released and the spectral data need not be stored, all other datafiles than xyzxyz.txt (where xyzxyz denotes the six-character name of the data) can be deleted. This file contains the summary of the SNR-data. However, other information is lost, and the data must then be viewed using a text editor.

• If the user wishes to keep the data needed for viewing them in the basic FluoroQuality form, the files xyzxyz.txt, xyzxyzsg.ave, xyzxyzsg.nps, xyzxyzsg.np1, xyzxyzbg.ave, xyzxyzbg.nps, xyzxyzbg.np1 and xyzxyzSNRdataonform.dat must be kept. If the files xyzxyzSNRsp.dat and xyzxyzSNR0sp.dat are deleted, the SNR-spectra shown on the form will be the biased spectra (this will be noted to the user by a text appearing below the spectrum).

• If the user wishes to be able to view the spatio-temporal NPS, the files xyzxyzsg.spt and xyzxyzbg.spt must be kept.

• If the user wishes to be able to view the original images and/or to be able to recalculate the results, the files xyzxyzPM.dat, xyzxyzYY.ims and xyzxyzYY.imt must be kept (YY is 01 – *M*, where *M* is the number of image sequences).

The contents of datafiles

• Average image data are saved as \AnalysedData\xyzxyzsg.ave and \AnalysedData\xyzxyzbg.ave for the signal and background sets, respectively. The files contain the pixel values as eight-byte real numbers, line by line, starting from the left upper corner.

• The temporal 0-frequency NPS of the signal and background image sets are saved as \AnalysedData\xyzxyzsg.nps and \AnalysedData\xyzxyzbg.nps. The files contain the NPS values as eight-byte real numbers, line by line, starting from the (0, 0) frequency[*)].

• The one-frame NPS of the signal and background image sets are saved as \AnalysedData\xyzxyzsg.np1 and \AnalysedData\xyzxyzbg.np1. The files contain the NPS values as eight-byte real numbers, line by line, starting from the (0, 0) frequency.

[*)] The origin of Fourier transformed data that are displayed on the form is in the middle of each image. In the data files the origin can be thought of as being located in the upper left corner. Note the periodicity of the DFT data.

- SNR measurement data is saved in the text file \AnalysedData\xyzxyz.txt.
- The SNR data displayed above the memo box in the basic form are contained in the text file \AnalysedData\xyzxyzSNRdataonform.dat.
- The spatio-temporal NPS for the signal and background data sets are saved in files \AnalysedData\xyzxyzsg.spt and \AnalysedData\xyzxyzbg.spt. The files contain the minimum and the maximum value of the data, the temporal sequence length and the NPS values as eight-byte real numbers. The data for each temporal frequency are written line by line each temporal frequency data starting with the spatial (0, 0) frequency, and the data are written for each positive temporal frequency.
- The file \AnalysedData\xyzxyzSNRsp.dat contains the spatial frequency components of the de-biased SNR^2-spectrum of single frames. These data are shown in the SNR^2(one frame) image on the basic form display. The file contain the values as eight-byte real numbers, line by line, starting from the (0, 0) frequency.
- The file \AnalysedData\xyzxyzSNR0sp.dat contains the spatial frequency components of the de-biased SNR^2_{rate}-spectrum. These data are shown in the SNR^2(0 Hz) image on the basic form display. The file contains the values as eight-byte real numbers, line by line, starting from the (0, 0) frequency.
- The text file \AnalysedData\xyzxyzSNR1280.dat contains the decision variable values of the direct one-frame SNR-measurement: the values refer to image files 1-*M* and are given for each frame. Signal case data first.
- The text file \AnalysedData\xyzxyzSNRSEQ1280.dat contains the decision variable values of the direct average-frame SNR-measurement method: the values refer to image files 1-*M*. Signal case data first.

APPENDIX D: THE FILES AND FILE FORMATS REQUIRED FROM THE ACQUISITION PROGRAM

The acquisition program must produce a set of files whose contents are described below. The measurement data consist of an acquisition parameter file, *M* image files for the signal and *M* image files for the background. The data for each separate measurement is identified by an arbitrary six-letter name which is being denoted below as “xyzxyz”.

The acquisition parameter file *PM.DAT

The acquisition parameters are stored in file whose name is xyzxyzPM.dat (replace xyzxyz by the name you wish to use). This file must contain seven data lines:

- The first line must contain an integer number (intended to show the opening mode of the frame grabber board, if there are variable modes of operation) – this datum is not actually used in the program, but is printed in the output data file xyzxyz.txt only. After the datum, the row may contain also an explaining text that is not being used in the program. In order to ensure compatibility with future versions of FluoroQuality we suggest that the number 0 is input here.
- The second line must contain the actual duration of each image sequence in centiseconds (For example, the duration of the 32 frames in a 50 Hz TV-chain is 32*40 ms = 128 cs). After the datum, the row may contain also an explaining text that is not being used in the program.
- The third line must contain the number of recorded sequences (denoted as *M* in chapter 3). After the datum, the row may contain also an explaining text that is not being used in the program.
- The fourth line must contain two integer numbers. The numbers represent the horizontal and vertical position of the analysed sub-image. The data are not actually being used in the program, but are shown in the output data file xyzxyz.txt only. After the datum, the row may contain also an explaining text that is not being used in the program.
- The fifth line must contain two integer numbers. The numbers represent the offset and white reference settings of the frame grabber board. The data are not actually being used in the program, but are shown in the output data file xyzxyz.txt only. After the datum, the row may contain also an explaining text that is not being used in the program.

- The sixth line contains a comment text that the user wishes to be shown in the output data file xyzxyz.txt.
- The seventh line contains the name of the acquisition program.

An example of the file xyzxyzPM.DAT is shown below:

```
0              ,  opening mode (dummy)
128            ,  cs, collection time
40             ,  number of series
339            251           , subimage location (dummy)
60             240           , offset, reference (dummy)
This is an example of a comment line
NoiseAcquisition
```

The image files *yy.ims and *yy.imt

The actual image data corresponding to the situation of the signal being in the image are written in *M* image data files whose names must be xyzxyz01.ims, xyzxyz02.ims, ...xyzxyz40.ims. (In this example *M* is 40.) The image data corresponding to the signal-absent-case are written in files xyzxyz01.imt, xyzxyz02.imt, ...xyzxyz40.imt. (In this example *M* is again 40.)

The pixel values are written, line by line, as bytes, beginning from the upper left corner of the first image in the sequence until all lines and all frames have been written. In Fortran, the code for writing the pixel values $g(i, j, k)$ of a sequence in the file xyzxyz01.ims is

```
      INTEGER*1 g(64,64,32)
...
      NAME='xyzxyz01.ims'
      OPEN(1, FILE=NAME, STATUS='NEW', RECL=64,
       FORM='UNFORMATTED')
      DO 2 K=1,32
      DO 2 J=1,64
2     WRITE(1) (g(I,J,K),I=1,64)
      CLOSE(1)
```

Here, *I* refers the horizontal location of the pixel, *J* the vertical location and *K* the frame. Note that in Fortran each file is started with a value 75 (denoting the beginning of the file) and ended with the value 130 (denoting the end of the file). Also, the length of the physical record is written at the beginning and end of each record : therefore, the actual record length here is 64+2 = 66 bytes, and the total size of each of the image sequence files is then 32*64*(64+2)+2 = 135 170 bytes.

In FluoroQuality (written in Delphi Object Pascal) the image files (e.g., xyzxyz01.ims) are read by:

```
NAME:='xyzxyz01.ims';
Assignfile(D,NAME);
FileMode := 0;
Reset(D, 66);
for K:=1 TO 32 do
    begin
    for J:=1 TO 64 do
        begin
        BlockREAD(D,line,1) ;
        for I:=1 to 64 do
            begin
            g[I,J,K]:=line[I+2];
            end;
        end;
    end;
CLOSEfile(D) ;
```

Here, *D* is defined to be an untyped file, *g* is an Array[1..64,1..64,1..32] of byte and *line* is an Array[1..66] of byte.